GCM SIMULATIONS OF THE LIFE CYCLES OF THE 1988 US DROUGHT AND HEAT WAVE

M. J. Fennessy*, J. L. Kinter III*, L. Marx*,
E. K. Schneider*, P. J. Sellers** and J. Shukla*

*Center for Ocean-Land-Atmosphere Studies, Calverton, Maryland
** NASA Goddard Space Flight Center, Greenbelt, Maryland

21 August, 1994

ABSTRACT

A series of ensemble integrations with the Center for Ocean-Land-Atmosphere Studies (COLA) model are conducted to determine the impact of observed global SST and a proxy observed global soil wetness initial condition on the initiation, maintenance and decay stages of the life cycles of the 1988 U.S. drought and heat wave, which were unusual compared to historical U.S. drought and heat wave life cycles. The results from these experiments are carefully compared to the observed anomalies and to the results of previously published studies, which focused on the time-mean drought and heat wave, rather than on their life cycles.

The prescribed time-varying observed global SST is found to be capable of forcing the initiation of the drought during April, given a SST analysis which accurately describes the strong negative SST anomalies observed in the eastern equatorial Pacific. In agreement with previously published studies, the observed global SST is also found to contribute to the drought maintenance during May and June. The proxy observed initial soil wetness also contributes to the drought maintenance during June. The SST and the initial soil wetness both contribute to the heat wave life cycle from June through July, but fail to force the month to month variability observed. Neither the SST nor the soil wetness anomalies appear to be responsible for the drought decay in early July. An important role for the internal dynamics of the atmosphere in forcing this month to month variability, as well as the drought decay is suggested. Important interactions between the SST and soil moisture forcing are noted, and the need for a soil moisture data set based on observations is emphasized.

1. Introduction

During April, May, and June (AMJ), 1988, widespread severe atmospheric drought conditions (negative precipitation anomalies) existed over much of the eastern and central United States (Janowiak, 1988; Ropelewski, 1988; Trenberth et al., 1988; Heim, 1990). The primary corn and soybean belt of the U.S. experienced the driest April-June growing season on record (Heim, 1990). Concurrently, anomalously strong upper level anticyclonic conditions occurred over North America which are closely associated with the surface drought conditions (Klein, 1990). The anomalous anticyclonic conditions over North America persisted throughout April, May and June, but reached a peak magnitude during June, at which time the 300 mb geopotential height anomaly exceeded 150 meters. Although the precipitation in this region returned to normal by July, the drought was followed by dry soil conditions and an intense heat wave over much of the U.S., which persisted throughout June, July, and August (JJA), 1988 (Ropelewski, 1988; Heim, 1990). For the U.S. as a whole, JJA 1988 was the third warmest summer on record (Heim, 1990).

The 1988 U.S. drought and heat wave were unusual in several respects. The location of the drought was displaced eastward of the more typical Great Plains droughts, such as occurred during the 1930's and 1950's. The boreal spring timing of the drought was unusual compared to most historical U.S. droughts, which more typically have occurred during boreal summer. The severity of the drought was also unusual. And although the upper-level atmospheric pattern of an anticyclone over the central U.S. flanked by troughs off either coast which accompanied the drought was characteristic of past U.S. drought patterns (Namias, 1991), its occurrence during boreal spring was unusual. The boreal summer heat wave was exceptional in its severity and is

unique in that the area of the most extreme temperature anomalies spanned the country from east to west (Ropelewski, 1988). The heat wave was also unusual in that the monthly surface temperature anomalies displayed large spatial variability. The region of maximum surface temperature anomalies was positioned over the upper midwest during June, over the extreme west and northeast during July, and over the central and eastern U.S. during August (see Ropelewski, 1988).

Preceding and concurrent with the drought and heat wave, significant anomalies were observed in the global sea surface temperature (SST) in several regions. In the central and eastern tropical Pacific, warm (El Niño) SST anomalies lasted until March, after which cold (La Niña) SST anomalies persisted throughout the remainder of the year. Kousky (1990) suggested that the poleward spread of anomalously warm tropospheric temperatures associated with an El Niño may be an important ingredient in helping to maintain mid-latitude upper tropospheric ridges at time-lags as great as 10 months after the maximum tropical SST is observed. Thus, although cold (La Niña) SST anomalies were observed at the time of the drought, it is possible that the preceding warm tropical SST conditions were a factor in setting up the circulation responsible for the drought. This concept is consistent with the results of Namias (1991), who suggested that antecedent atmospheric, soil and SST conditions set up the circulation pattern associated with the drought, and that the drought may have been predictable from as early as March, 1988.

Trenberth et al. (1988, hereafter TBA) analyzed the atmospheric circulation patterns observed during May and June 1988 and identified patterns in the anomalous 500 mb geopotential height resembling dispersion of Rossby waves emanating from the central and

eastern tropical Pacific towards the northeast Pacific and North America. A strong ridge over the central U. S. related to the downstream surface drought conditions was one part of this pattern. TBA forced a simple atmospheric model with idealized heating anomalies derived from the anomalous outgoing longwave radiation (OLR) observed in the eastern tropical Pacific during May and June 1988, and obtained a wave train over the Pacific and North America resembling that observed. The anomalous OLR signal used represented a convective heating anomaly dipole in the eastern Pacific, corresponding to a negative precipitation anomaly along the equator and a positive precipitation anomaly in the vicinity of 10°N. Given the well known link between tropical SST and convective heating, TBA hypothesized that the SST anomalies in the tropical Pacific forced an anomalous Rossby wave train which resulted in upper level ridging over the central U. S. and drought conditions below.

In a continuation of the research of TBA, Trenberth and Branstator (1992) presented further diagnostic and model calculations with important implications for general circulation model (GCM) studies. They forced the same model used by TBA with idealized versions of diagnosed May 1988 heating anomalies over 10 different regions. Only the heating anomalies corresponding to the observed anomalies in the eastern tropical Pacific forced a response over North America similar to that observed, thus lending support to the conclusion of TBA. However, their diagnostic and model calculations showed that "feedback-caused soil moisture anomalies may have been secondary sources for the drought circulation". Trenberth and Branstator also emphasized the importance of using realistic SST in attempting to simulate the drought with GCMs, noting the weakness of the April 1988 eastern equatorial Pacific negative SST anomalies in one widely used analysis.

Following the study by TBA, several atmospheric GCM simulation studies have investigated the 1988 U. S. drought, including Palmer and Branković (1989), Branković et al. (1990), Fennessy et al. (1990), Mo et al. (1990, 1991), Sud et al. (1990), Sugi et al., (1990), and Atlas et al. (1993).

Palmer and Branković (1989) compared two 30 day mean forecasts with the European Center for Medium-Range Weather Forecasts (ECMWF) GCM initialized in mid-June 1987 and 1988, both using global SST observed at the time of initialization. They found that the GCM simulated some of the observed interannual variability, including increased 300 mb geopotential heights and reduced precipitation over the U.S. in 1988 versus 1987. The 1988 integration was repeated using the 1987 SST originally used in the 1987 integration. A comparison of the three integrations revealed that much of the correctly simulated interannual variability was due to the SST boundary condition. They concluded that the anomalous SST in 1987 and 1988 was important in accounting for the reduction in rainfall over the U.S. in the summer of 1988.

Branković et al. (1990) conducted a number of 90-day integrations with a T42 version of the ECMWF GCM initialized from 1 March, 1 April, 1 May and 1 June 1988, using both climatological and observed SST globally. These integrations included 2 levels of prognostic soil moisture which were initialized with real-time values from the ECMWF analysis-forecast system. An additional integration initialized from 1 June 1988 was done in which the soil moisture throughout the course of the integration was set to seasonally varying climatological values. Branković et al. (1990) examined mainly seasonal means, in agreement with the argument put forth by Palmer (1987), that with longer time scales internal atmospheric variability decreases and the proportion of variability due to boundary forcing increases. Comparing integrations with

observed versus climatological SST, they found an increase in both the strength and veracity of the simulated seasonal mean 200 mb wavetrain across the Pacific and North America as the initial date of the integrations approached boreal summer. They also found that the veracity of the most successful seasonal integration (JJA), was highly dependent on using real-time rather than climatological soil moisture. They concluded that the late spring and summer SST anomalies played an important role in establishing anticyclonic conditions over the North American continent, but that the maintenance and decay of these conditions must be viewed in interaction with land surface processes. Their finding concerning the importance of soil moisture is in qualitative agreement with the results of Oglesby (1990, 1991), who found that mid-to-late spring soil moisture could have a significant impact on the North American climate the following summer in experiments done with the National Center for Atmospheric Research (NCAR) CCM1 GCM.

Mo et al. (1990, 1991) used a T40 version of the National Meteorological Center (NMC) medium-range-forecast model (MRF) to study the relative importance of using realistic SST versus that of using a realistic initial atmospheric state in simulations of the drought circulation of June 1988. They found that control integrations initialized from 21, 22, and 23, May 1988, using climatological SST as a global boundary condition produced reasonable simulations of the drought circulation during June. The same integrations repeated with observed global SST produced an even more realistic drought simulation. They concluded that the observed SST contributed to, but did not solely cause the 1988 U.S. drought during June, 1988.

Sud et al. (1990) used the 4° latitude by 5° longitude Goddard Laboratory for Atmospheres (GLA) GCM to investigate the influence of observed SST during June and July, 1988. They

performed integrations initialized from 00 UTC 19 May, 12 UTC 19 May, and 00 UTC 20 May, 1988 with both climatological and observed global SST. They found some consistent resemblance between the mean observed and simulated circulation fields over North America, but little statistical significance or correspondence between the anomalies observed and those simulated in response to the observed SST. They concluded that the model failed to simulate significant circulation features that are clearly associated with the drought.

Sugi et al. (1990) analyzed June 1988 integrations using observed global SST with both the Meteorological Research Institute (MRI) 4° latitude by 5° longitude GCM and a T63 version of the Japan Meteorological Agency (JMA) GCM. They found that both GCMs under-forecast the strength of the mid-latitude stationary waves in general, and of the anomalously strong anticyclonic conditions over North America, in particular. Comparing the MRI GCM results to integrations done using global climatological SST, they found little impact of the observed SST on the simulation in the drought region. Additional integrations done using idealized eastern tropical Pacific heating anomalies similar to those used by TBA yielded a stronger, but still weak response over North America.

Fennessy et al. (1990) analyzed 60-day integrations from two different GCMs done with both global climatological and global observed SST, initialized from 1, 2, and 3, May 1988. One GCM used was an old version of the Goddard Laboratory for Atmospheric Sciences (GLAS) GCM, which is a 4° x 5° grid point model with 9 vertical levels. The other GCM used is a version of the Center for Ocean-Land-Atmosphere Studies (COLA) GCM, which uses spectral dynamics with rhomboidal truncation at wave number 40, and has 18 vertical levels. Fennessy et al. compared the May-June (MJ) time mean circulation features of these two GCMs which they

believed were relevant to the 1988 U.S. drought, to observations. They found that the veracity of the COLA GCM in simulating these time mean features appeared to be sufficient for studying the 1988 U.S. drought, but that the veracity of the GLAS GCM was not. A summary of key mean and anomalous circulation features which GCMs must successfully simulate to properly study possible drought mechanisms is given by Trenberth (1990) and Trenberth and Branstator (1992).

Fennessy et al. (1990) did obtain a wavetrain pattern emanating from the eastern tropical Pacific similar to that of TBA in response to using the observed 1988 SST with the COLA GCM, however the pattern was weak and eastward shifted compared to that observed. Thus, the associated region of maximum rainfall reduction was over the Gulf Stream, eastward of that observed in the central and eastern U.S. They concluded that the anomalous SST observed in the Pacific may have enhanced, but not solely caused the 1988 U.S. drought during MJ 1988. However, they also noted that vorticity source diagnostics appeared to indicate extra-tropical forcing due to anomalous SST in other regions of the tropics, and emphasized the need for a careful diagnosis of the physical mechanisms operating in the GCM response to observed SST.

Atlas et al. (1993) used the Goddard Laboratory for Atmospheres (GLA) 4° latitude by 5° longitude GCM to examine the impact of observed SST and soil moisture anomalies on simulations of the Great Plains region of the U.S. during May and June, 1988. They found that the 1988 tropical SST anomalies significantly reduced the Great Plains precipitation, but that the 1988 midlatitude SST anomalies did not. Their use of proxy 1988 soil moisture anomalies resulted in larger precipitation anomalies than obtained in the SST experiments, as well as significant surface temperature anomalies over the Great Plains region.

The preceding GCM studies suggest possible roles for both SST and soil moisture forcing of the U.S. drought and heat wave during the late spring and summer of 1988. They also clearly show the importance of having a reasonable mean circulation before attempting to simulate the response to anomalous boundary conditions. However, these studies do not directly address the issue of just how important anomalous boundary forcing was on the life cycle of the drought, and particularly do not address the role of boundary forcing during either the initiation or the decay of the drought. These studies also fail to address the role of boundary forcing regarding the observed time lag between the drought (precipitation deficit) which occurred during AMJ, and the heat wave which occurred during JJA and exhibited considerable spatial variability from month to month. The goal of the current study is to further our understanding of the entire life cycle of the 1988 U. S. drought and heat wave by examining the possible role of forcing by global SST and global soil moisture. A recent version of the COLA GCM has been used to investigate (1) the impact of observed global SST on the life cycles of the U.S. drought and heat wave from April through August 1988, and (2) the influence of a proxy observed global soil moisture initial condition on the life cycles of the drought and heat wave from June through August, 1988.

As shown by TBA and others, the rainfall deficit over the eastern U.S. began in April. The previously discussed GCM studies have not separately addressed the impact of SST during this initiation stage of the drought. The work of Lau and Peng (1990, 1992) suggests that it may be unlikely that the tropics could force the mid-latitude circulation over North America at this time. Their wave flux computations for the climatological flow suggest that tropical forcing has little influence on the summertime planetary scale circulation over the Pacific/North America

region until the month of June. Because the 1988 U.S. drought was well underway by June, they hypothesized that tropical forcing could have amplified the drought, but could not be responsible for its initiation. Moreover, calculations of the anomalous flux of stationary wave activity (Plumb, 1985) by Lyon (1991) indicate that the anomalous wave activity during AMJ 1988 emanates from the western North Pacific rather than from the tropics. Thus, the role of SST forcing during the U.S. drought initiation in April remains an open question which we address in this study.

Given the highly unusual life cycles of the drought and the heat wave a thorough examination of the role of boundary forcing on each phase of these life cycles is in order, and is attempted here. The model formulation and experimental design are outlined in section 2. The impact of global SST on the initiation of the drought in April, 1988 is discussed in section 3. The impact of global SST on the life cycle of the drought and heat wave from May through August, 1988 is discussed in section 4. The impact of global soil wetness on the final stages of the atmospheric drought and the life cycle of the heat wave during June, July and August is discussed in section 5. A summary is given in section 6.

2. Model and experimental design

a Model

The COLA GCM is based on a modified version of the NMC global spectral model used for medium range weather forecasting (see Sela, 1980 for original NMC formulation; see Kinter et al., 1988 for the modified version). The land surface parameterization was changed to the

Simple Biosphere model (SiB) biophysical formulation after Sellers et al. (1986) by Sato et al. (1989a) and later simplified by Xue et al. (1991). The model used in most of these experiments is the same as the mean orography version presented by Fennessy et al. (1994).

The COLA GCM is a global spectral model with rhomboidal truncation at zonal wave number 40. The model physical calculations are done on a 1.8° latitude by 2.8° longitude Gaussian grid. The vertical structure of the model is represented by 18 unevenly spaced levels using sigma as the vertical coordinate (Phillips, 1957). The spacing of the levels is such that greater resolution is obtained near the earth's surface and at the tropopause. In addition to the parameterizations mentioned above, the COLA GCM includes parameterizations of solar radiative heating (Lacis and Hansen, 1974), terrestrial radiative heating (Harshvardhan et al., 1987), deep convection (Anthes, 1977; after Kuo, 1965), shallow convection (Tiedke, 1984), large scale condensation, interactive cloud-radiation (Hou, 1990; after Slingo, 1987), gravity wave drag (Vernekar et al., 1992; after Alpert et al., 1988) and a turbulence closure scheme for subgrid scale exchanges of heat, momentum and moisture (Miyakoda and Sirutis, 1977; Mellor and Yamada, 1982).

All the integrations presented here were conducted using the recent version of the COLA GCM described above and used by Fennessy et al. (1994) except for the integration ensembles initialized from 1, 2, 3 April 1988 (see Table 1). The model used in the latter ensembles is a previous version which used the full SiB (Sellers et al., 1986) rather than the simplified SiB (Xue et al., 1991), used a silhouette rather than a mean orography (Fennessy et al., 1994), and did not include a parameterization for gravity wave drag. Ensemble boreal summer simulations done with these two versions of the COLA GCM are very similar over North America. However, both

versions yield better monthly and seasonal simulations than the COLA GCM used by Fennessy et al. (1990), which included a simple bucket hydrology rather than SiB, predicted moisture at only the lowest 12 sigma levels and used prescribed seasonally varying zonally symmetric clouds in the radiative heating calculations.

Before we can expect a GCM to correctly simulate the effects of anomalous forcing on the atmosphere, the GCM must first do a reasonable job of simulating the relevant mean features of the atmospheric circulation (Fennessy et al. 1990, Trenberth 1990, Trenberth and Branstator, 1992). We have examined the time mean simulations from the COLA GCM used here, and believe that the GCM produces reasonable enough simulations of the relevant time mean observed atmospheric circulation features to be used for this study. These relevant features include the time mean tropical precipitation, heating and divergence, the northern hemisphere three dimensional horizontal wind and geopotential height and the North American precipitation. For the sake of brevity we will not show all these mean fields here, but will refer to veracity of relevant features when necessary.

b. Experimental design

A series of experiments consisting of COLA GCM integration ensemble pairs was conducted to determine what role forcing by global SST and global soil wetness played in the life cycles of the drought and heat wave. A summary of the integration ensemble names, integration initiation dates (all 00UTC and 1988), integration lengths, SST boundary condition used and soil wetness initial condition used is given in Table 1.

Ensemble name	Initiation dates	Length (days)	SST	Soil wetness IC
MARCLSST	1, 2, 3 March	60	Climatological*	Climatological+
MAROISST	1, 2, 3 March	60	1988 OI**	Climatological+
APRCLSST	1, 2, 3 April	90	Climatological*	Climatological+
APRBLSST	1, 2, 3 April	90	1988 Blended***	Climatological+
JUNCLSST	1, 2, 3 June	90	Climatological*	Climatological+
JUNBLSST	1, 2, 3 June	90	1988 Blended***	Climatological+
JUNBLSSTSW	1, 2, 3 June	90	1988 Blended***	1988ECMWF++
JUNCLSSTSW	1, 2, 3 June	30	Climatological*	1988ECMWF++

TABLE 1. Integration ensemble names, initiation dates, lengths, SST used (*Reynolds (1988), **Reynolds and Smith (1994), ***Reynolds (1988)) and soil wetness initial condition (IC) used (+from Willmott et al. (1985), ++from 1 June ECMWF analysis-forecast cycle soil moisture).

To investigate the impact of global SST on the drought initiation, integration ensembles were conducted with the COLA GCM using both climatological SST and observed SST, initialized from observed analyses of the atmospheric state during early boreal spring, 1988. The

April 1988 SST impact was first tested in a pair of integration ensembles. (APRCLSST, APRBLSST) initialized from early April in which the observed SST ensemble uses the SST analysis of Reynolds (1988). Following the concerns of Trenberth and Branstator (1992) regarding the weakness of the April SST anomalies inherent in this analysis, a second pair of integration ensembles (MARCLSST, MAROISST) were initialized from early March 1988, in which the observed SST ensemble uses a new high resolution weekly global SST analysis (Reynolds and Smith, 1994) which is more in accord with the April 1988 buoy data cited by Trenberth and Branstator (1992).

To investigate the impact of global SST on the drought maintenance during May and June, the decay of the drought by July, and the life cycle of the heat wave from June through August, two sets of 90 day integration ensemble pairs done with the COLA GCM are analyzed, each pair consisting of a climatological SST ensemble and an observed SST ensemble, initialized from observed analyses of the atmospheric state during early April 1988 (APRCLSST, APRBLSST) , and early June 1988 (JUNCLSST, JUNBLSST), respectively.

To determine the role of soil wetness in the life cycle of the 1988 U.S. drought and heat wave we examined the GCM interaction with the soil wetness, which has not been observed. Initialization and validation of GCM soil wetness fields has long been recognized as a challenging problem (Sellers et al. 1986, 1989; Sato et al. 1989a, 1989b). It should be possible to initialize GCM integrations with observed soil moisture data obtained through the use of a hybrid methodology incorporating remotely sensed data with sophisticated coupled atmosphere-biosphere models (Sellers, 1990; Liston et al., 1993). As this sort of hybrid soil wetness data is not yet available, we study the impact of initializing the COLA GCM with proxy observed 1988

soil wetness derived from the prognostic soil moisture which is produced by the ECMWF operational analysis-forecast cycle.

Calculations with a modified version of the Ceres-Maize corn growth model (Kunkel, 1990a) have shown that crops in the vicinity of Champaign, Illinois, located in the middle of the corn belt where the AMJ precipitation deficit occurred, were not under stress due to lack of moisture until early June, 1988 (Kunkel, personal communication, 1994). Measurements taken from 30 June through 18 August 1988, at a site near Champaign, Illinois, show that crops were under stress due to lack of moisture by late June, 1988 (Kunkel, 1990b). To study the influence of soil wetness on the 1988 U.S. drought and heat wave, we compare two 90-day GCM ensembles initialized in early June, one initialized with climatological soil wetness (JUNBLSST) and the other initialized with proxy observed 1988 soil wetness (JUNBLSSTSW). Each of these ensembles use observed SST (Reynolds, 1988). This experiment differs from that done by Branković et al. (1990), because we performed an ensemble, rather than one integration pair, and because, after initialization, we allowed the GCM to predict soil wetness via the use of a sophisticated hydrological/biosphere model. Atlas et al. (1993) also used fixed, non-interactive soil moisture anomalies in their May-June experiments, and focused their analysis on the Great Plains region which lies west of the area of large precipitation anomalies observed during AMJ 1988. By imposing only initial proxy observed soil wetness anomalies and using interactive soil wetness in our experiments, we can more directly address the question of whether the June precipitation deficit and the JJA heat wave were caused or augmented by soil wetness anomalies set up by the preceding dry spring. In addition, the use of interactive soil wetness allows us to study how SST forcing impacts the evolution of the soil wetness . To investigate the

independence of the SST forcing and the soil wetness forcing, a final ensemble is integrated for the month of June which is initialized with the proxy observed 1988 soil wetness but uses climatological SST (JUNCLSSTSW).

3. Impact of SST on drought initiation during April

a. Early April initial conditions SST experiment

Three COLA GCM 90-day integration pairs were initialized from the NMC analyses of the observed atmospheric states at 0000UTC on 1, 2, and 3 April 1988. Each pair consists of a control integration with global time-varying climatological SST specified ("COADS/ICE Blended Climatology", Reynolds and Roberts, 1987) and an integration with global time varying observed SST for 1988 ("Blended Analysis", Reynolds, 1988). Although both SST analyses are monthly, the model interpolates the SST to daily values during integration. The ensemble means will be referred to as APRCLSST and APRBLSST, respectively. The integrations are initialized with calculated climatological soil wetness (Willmott et al., 1985). In all the integrations presented in this paper the SiB model predicts the soil wetness after initialization.

The monthly anomalies formed by subtracting the 1988 Blended Analysis from the climatology are shown for March, April and May, 1988 in Figs. 1a-c respectively, plotted on the 2° x 2° grid on which both SST analyses originate. The SST in the eastern equatorial Pacific changes from warm El Niño conditions in March (Fig. 1a), to weak cold La Niña conditions in April (Fig.1b), to strong cold La Niña conditions in May (Fig. 1c). The integration ensembles were initialized in early April to investigate the possible impact of this cold La Niña SST anomaly on the GCM simulation of the initiation of the 1988 U.S. drought in April. We should

note that in this and all other experiments presented here, global SST was specified, so it is possible that SST forcing from regions other than the eastern equatorial Pacific may affect the simulated North American climate, as pointed out by Fennessy et al. (1990). However, the calculations of Trenberth and Branstator (1992) suggest that during AMJ 1988, only the observed heating anomalies in the eastern tropical Pacific were capable of forcing an anomaly signal similar to that observed over North America. Our emphasis will be on the SST forcing from this region.

The April mean observed precipitation anomaly is shown in Fig. 2a. This and all other observed precipitation anomalies shown in this paper were computed as the difference between the observed monthly 1988 precipitation and the observed monthly climatological precipitation. The observed monthly 1988 precipitation was computed by combining the Global Precipitation Climatology Center (of the Global Precipitation Climatology Project, Janowiak and Arkin, 1991) gridded station data over land, and precipitation derived from the Microwave Sounding Unit (MSU) satellite data over ocean (Spencer, 1993). The observed monthly climatological precipitation was computed by combining the 1979-1993 gridded precipitation climatology over land derived from the NMC Climate Analysis Center (CAC) Climate Anomaly Monitoring System station data archive (CAMS, Ropelewski et al., 1985) with a 1979-1991 precipitation climatology over ocean calculated from the MSU satellite precipitation data (Spencer, 1993). During April 1988 a 2 mm day^{-1} negative anomaly centered on the equator extended from 150°W to 80°W, and a 1-2 mm day^{-1} positive anomaly centered at 8-10°N extended from 150°W to 120°W (Fig. 2a). The APRBLSST - APRCLSST ensemble mean April 1988 mean precipitation anomaly included a similar statistically significant anomaly dipole in the eastern tropical Pacific,

although both simulated anomalous centers were approximately 2° north of those observed and the positive anomaly was centered 15° east of that observed (Fig. 2b). On all the simulated ensemble anomaly maps presented in this paper the regions where the ensemble anomaly was significant at the 95% confidence level as determined by a student's t-test are denoted by shading.

The 1988 U.S. drought may be defined as the region of the 1 mm day^{-1} negative anomaly which extended southward from the western portion of the Great Lakes (Fig. 2a). A region roughly three times this size was encompassed by the -0.5 mm day^{-1} contour (not drawn on Fig 2a). The wave train link envisioned by TBA between the tropical precipitation anomalies and the U.S. precipitation anomalies depicted in Fig. 2a can be seen in the observed 300 mb geopotential height anomaly for April 1988 (Fig. 2c). This and all other observed 300 mb geopotential anomalies shown in this paper were computed by subtracting the mean monthly climatology for 1980-1992 calculated from ECMWF analyses from the monthly mean of the ECMWF analyses for 1988. The APRBLSST - APRCLSST ensemble mean April 1988 mean 300 mb geopotential height anomaly does not show a similar wave train, bears no resemblance to the observed height anomaly over the eastern Pacific and North America, and includes no statistically significant signal over North America (Fig. 2d). No significant precipitation anomalies were simulated over the U.S. during April, and the (statistically insignificant) signal in the Great Lakes region is of the wrong sign (Fig 2c). An examination of the individual April mean APRBLSST - APRCLSST ensemble members reveals that none of the three contain precipitation anomalies or 300 mb geopotential anomalies similar to those associated with the U.S. drought (not shown). The shading of the entire tropics up to about 20°N in Fig. 2d is indicative of the small, but reproducible, positive geopotential height anomalies which are

indicative of a slightly warmer tropical troposphere in the APRBLSST ensemble. This feature may be seen in all the observed minus climatological SST 300 mb geopotential height anomaly maps depicted in this paper, indicating a tendency for a slightly warmer tropical troposphere in observed SST versus climatological SST integrations.

b. SST considerations

The results from this pair of integration ensembles indicate that the SST related tropical heating anomalies observed during April 1988 were not responsible for initiating the 1988 U.S. drought. However, motivated by the doubts raised by Trenberth and Branstator (1992) concerning the weakness of the eastern equatorial Pacific April 1988 SST anomalies inherent in the Blended SST analysis of Reynolds (1988), which was used in the APRBLSST ensemble, we examined a more recently available high resolution (1° x 1°), weekly SST optimal interpolation analysis (hereafter OI SST, Reynolds and Smith, 1994). The March, April and May 1988 SST anomalies computed by subtracting the monthly Reynolds and Roberts (1987) climatology from monthly means calculated from the 1988 weekly OI SST analyses of Reynolds and Smith (1994) are shown in Figs. 3a, 3b and 3c respectively, plotted on the 2° x 2° grid used for the climatology. We compare these anomalies to those formed by subtracting the same climatology from the Blended SST analyses of Reynolds (1988) depicted in Figs 1a, 1b and 1c, and focus on the eastern tropical Pacific. The March 1988 OI SST anomalies (Fig 3a) contain a narrow band of small (0.5°C) anomalously negative SST along the equator in the eastern tropical Pacific not found in the corresponding Blended SST anomaly (Fig. 1a). During April 1988, the OI SST negative anomaly in the eastern equatorial Pacific reaches 1-2°C (Fig. 3b), whereas the

corresponding Blended SST anomaly reaches only 0.5-1°C (Fig. 1b). The April 1988 difference map between these two figures (1b and 3b) reveals a 1°C or greater difference along the equator from 135°W to 90°W (not shown). Also notable in both March and April is the considerably weaker warm anomaly just north of the equator in the vicinity of 120°W in the OI SST (about 0.5°C) compared to the Blended SST (1°C or greater). The two analyses of the anomaly in the eastern tropical Pacific are much more similar during May (Figs 1c, 3c), and in the following months (not shown). An examination of the difference between the Blended SST analysis and the OI SST analysis for the months of March, April, May, June, July and August, 1988 reveals that the largest coherent difference between the two analyses in the tropics occurs in the eastern equatorial Pacific in April, 1988 (not shown). Thus, the conjecture of Trenberth and Branstator (1992) was corroborated.

The appearance of a negative anomaly in the March 1988 OI SST (Fig. 3a) suggests that the transition from warm to cold water in the eastern equatorial Pacific occurred before April, 1988. An examination of the weekly OI SST anomalies computed by subtracting the interpolated weekly climatological SST (derived from the monthly climatology of Reynolds and Roberts, 1987) from the weekly OI SST centered on 13, 20 and 27 March, 1988 respectively, suggests that the transition occurred between 13 March (Fig. 4a) and 20 March (Fig. 4b), and that by the week centered on 27 March, the cold eastern equatorial Pacific SST anomaly was well established (Fig. 4c). These cold conditions persisted throughout the remainder of the boreal spring and summer. Given the abrupt transition in March in the eastern equatorial Pacific found in the OI SST, including a much stronger April 1988 anomaly, another integration ensemble pair was initialized from early March 1988, with one pair of the ensemble utilizing the weekly OI

SST analyses, in order to more fairly test whether the observed SST could have forced the initiation of the U.S. drought in April.

c. Early March 1988 initial conditions SST experiments

Three COLA GCM 60-day integration pairs were initialized from the NMC analyses of the observed atmospheric states at 00UTC on 1, 2, and 3 March 1988. Each pair consisted of a control integration with specified global time-varying climatological SST (Reynolds and Roberts, 1987) and an integration with global time varying observed SST for 1988 (OI SST, Reynolds and Smith, 1994). Both the monthly climatological SST and the weekly 1988 OI SST are interpolated to daily values during integration. The ensemble means will be referred to as MARCLSST and MAROISST, respectively.

The April 1988 MAROISST - MARCLSST ensemble precipitation anomaly (Fig 5a) and ensemble 300 mb geopotential height anomaly (Fig. 6a) are compared to the April mean observed anomalies depicted in Figs. 2a and 2c, respectively, and the April mean APRBLSST - APRCLSST ensemble anomalies depicted in Figs. 2b and 2d, respectively. The negative precipitation anomaly in the eastern equatorial Pacific and the positive anomaly just to the north are both better represented by the MAROISST - MARCLSST ensemble (Fig. 5a). In particular, the position of the positive anomaly, centered at 135°W, is substantially better than the APRBLSST - APRCLSST positive anomaly position centered at 120°W, 15° to the east of that observed. However, both the negative and positive anomalies are still about 2° north of those observed. The MAROISST - MARCLSST April mean 300 mb geopotential height anomaly (Fig. 6a) contains a statistically significant wave train pattern appearing to emanate from the region

of the positive precipitation anomaly in the eastern equatorial Pacific which is similar to, but in general somewhat east of that observed (Fig. 2c). Part of this simulated wave train is a positive anomaly (ridge) over North America which is centered over the Hudson bay area, where it has a magnitude of 150 meters. The MAROISST - MARCLSST April precipitation anomaly has a negative 0.5 mm day^{-1} anomaly just south of the Great Lakes which is not statistically significant at the 5 % level (0.5 mm day^{-1} contour not shown). An examination of the individual members of the MAROISST-MARCLSST ensemble reveals considerable variability among the April mean 300 mb geopotential height anomalies initialized from 1, 2 and 3 March 1988 (Figs. 6b, 6c, and 6d respectively) and the corresponding April mean precipitation anomalies (Figs. 5b, 5c and 5d, respectively). Two of the three members contain good representations of the positive precipitation anomaly at 135°W, 12°N, strong wave trains, large positive 300 mb geopotential height anomalies centered over the Hudson Bay area, and negative precipitation anomalies of 1 mm day^{-1} or more in the observed drought region (Figs. 5b, 5d, 6b and 6d). The only ensemble member which contains a good representation of the phase of the entire wave train has the most realistic negative precipitation anomalies in the U.S. drought region (Figs 6b, 5b). This member also has the strongest positive precipitation anomaly at 135°W, 12°N (Fig. 5b). An analysis of the daily area averaged anomaly time series for each integration pair shows that the strength of the positive precipitation anomaly at 135°W, 12°N is well correlated with the occurrence and strength of the positive 300 mb geopotential height anomaly over North America (not shown).

Thus, it appears that the anomalous SST observed during April 1988 in the tropical eastern Pacific is capable of forcing the observed anomalous upper level wave train, and hence the initiation of the 1988 U.S. drought, in accordance with the hypothesis put forth by TBA.

However, even given a perfect forecast of the March and April SST, an ensemble of three integrations with an atmospheric GCM may not have been sufficient to have forecast the drought in advance.

4. Impact of SST on the drought and heat wave from May through August

To investigate the impact of global SST on the drought maintenance during May and June, the decay of the drought by July, and the life cycle of the heat wave from June through August, two sets of 90 day integration ensemble pairs done with the COLA GCM are analyzed. The last 60 days of the three 90-day integration pairs initialized on 1, 2, and 3 April 1988, and discussed in section 3a (APRCLSST and APRBLSST ensembles), are analyzed to determine the impact of the observed global SST during May and June. Three 90-day integration pairs initialized from the NMC analyses of the observed atmospheric states at 0000UTC on 1, 2, and 3 June 1988 are analyzed to determine the impact of the observed global SST during June, July and August. The ensembles of the integrations initialized in June will be referred to as JUNCLSST and JUNBLSST, respectively. The APRCLSST and JUNCLSST ensembles use global time-varying climatological SST (Reynolds and Roberts, 1987), and the APRBLSST and JUNBLSST ensembles use global time varying observed SST for 1988 (Reynolds, 1988). As discussed in section 3b, the tropical SST anomalies associated with the Reynolds (1988) SST analyses used in these integration pairs are very similar to the anomalies formed by using the newer high resolution OI SST analyses of Reynolds and Smith (1994) for the months of May through August, 1988. The Reynolds (1988) minus Reynolds and Roberts (1987) June, July and August 1988 SST anomalies are shown in Figs. 7a-c. The cold La Niña SST anomaly in the

eastern equatorial Pacific declines from its peak magnitude of roughly 3°C in June, but remains with reduced magnitude, throughout July and August. The positive SST anomaly to the north of the equator in the eastern Pacific is reduced in magnitude to roughly 0.5°C during JJA, compared to its magnitude of 1°C or more in the same analyses during March, April and May (Figs. 1a-c).

a Impact of SST on drought maintenance during May and June

The MJ mean APRBLSST-APRCLSST ensemble precipitation anomaly (Fig. 8b) correctly simulates the strong positive-negative anomaly dipole observed in the eastern tropical Pacific during MJ 1988 (Fig. 8a). The MJ mean APRBLSST-APRCLSST ensemble 300 mb geopotential height anomaly contains a statistically significant wave train arcing over North America (Fig.8d), which is similar to, albeit weak and somewhat eastward of that observed (Fig. 8c). Thus, a positive 300 mb geopotential height anomaly over North America is simulated downstream of the observed position. The Pacific-North America region height anomaly depicted in Fig. 8d is very similar to the MJ 300 mb geopotential anomaly from an ensemble integration pair initialized in early May 1988 by Fennessy et al. (1990, Fig. 6c), who used the same SST analyses as used here, but an earlier version of the COLA GCM than that used here. The only statistically significant APRBLSST-APRCLSST MJ mean precipitation anomaly simulated over the U.S. is well south of the main observed drought area (Fig. 8b).

An examination of the individual members of the APRBLSST-APRCLSST ensemble reveals considerable variability among the simulated MJ mean 300 mb geopotential height anomalies and the corresponding MJ mean precipitation anomalies (not shown). Two of the three

members contain good representations of the strong precipitation anomaly dipole observed in the eastern tropical Pacific and have wave trains in the 300 mb geopotential height which appear to emanate from this region. Of these two, one contains a wave train, a positive North American geopotential height anomaly and a negative precipitation anomaly very similar to those observed, and the other contains a wave train which is shifted 30° east of that observed over North America, and thus has geopotential height and precipitation anomalies of opposite sign of those observed in the drought area. The third ensemble member contains a weaker than observed precipitation anomaly dipole in the eastern tropical Pacific and has out of phase 300 mb geopotential height anomalies over North America that appear to be part of a wave train pattern originating from the western tropical Pacific or further west over southern Asia. All three ensemble members had 300 mb geopotential height anomalies that could be interpreted as wave trains originating from regions of the tropics other than the eastern Pacific, however the variability of these other wave train features was so great that they do not appear in the ensemble anomaly (Fig. 8d). The occurrence of such wave train features is in agreement with an analysis of the GCM simulated Rossby wave source (Sardeshmukh and Hoskins, 1988) by Fennessy et al. (1990), which revealed anomalous tropical vorticity sources associated with observed SST anomalies in several regions of the tropics during MJ 1988.

The separate May and June monthly mean anomalies have also been examined and compared to the observed anomalies. As a group, the APRBLSST-APRCLSST May and June ensemble anomalies, the Fennessy et al. (1990) May and June ensemble anomalies, and the JUNBLSST-JUNCLSST June ensemble anomalies, indicate that the SST forcing of the wavetrain and precipitation anomalies associated with the U.S. drought was similar in magnitude in May and June (not shown).

The MJ results presented here suggest that the GCM can simulate the observed wave train and contribute to the maintenance of the U.S. drought in response to the observed SST forcing from the eastern equatorial Pacific. However, as with the April results presented in section 3, the remote GCM response was sufficiently variable that an ensemble of three integrations was not sufficient to forecast the maintenance of the drought with a practically applicable degree of certainty.

b. Impact of SST on U.S. precipitation during July and August

Although dry soil conditions remained throughout the summer, the precipitation over the U.S. returned to relatively normal amounts in early July. The July-August mean (JA) observed precipitation anomaly retained a strong anomaly dipole in the eastern tropical Pacific, but there were no coherent precipitation anomalies over North America (Fig. 9a). The JA JUNBLSST-JUNCLSST precipitation anomaly contains a good representation of the observed anomaly dipole in the eastern tropical Pacific and contains no significant anomalies over North America except for a positive 0.5 mm day^{-1} anomaly over a small area in the vicinity of the Great Lakes (Fig. 9b, 0.5 mm day^{-1} contour not shown) where a 1 mm day^{-1} positive anomaly was observed (Fig.9a). Neither the observed nor the JUNBLSST-JUNCLSST ensemble 300 mb geopotential anomalies have strong features over North America during JA 1988 (Figs. 9c and 9d, respectively). This absence of observed and simulated anomalies over North America is also evident in the individual July and August monthly mean precipitation and 300 mb geopotential height anomalies (not shown).

c. Impact of SST on heat wave during June, July and August

The heat wave which was observed over the U.S. during JJA 1988 changed considerably from month to month. The observed surface temperature anomalies shown in this paper were computed by taking the difference between the observed 1988 monthly surface temperature and the observed 1979-1993 monthly climatological surface temperature, both of which were derived from the CAC CAMS station data archive (Ropelewski et al., 1985). During June, large surface temperature anomalies of up to 5°C were observed over and to the north of the U.S. Great Plains region (Fig. 10a), located beneath the large 300 mb geopotential anomalies observed during June (Fig. 14b). During July, positive surface temperature anomalies of 1-2°C occurred in a 10° latitude wide horseshoe shaped band across the northern U.S., with maxima of 2°C near both coasts (not shown). During August, 1-2°C surface temperature anomalies covered the eastern half of the U.S., with a maximum greater than 2°C centered just south of the Great Lakes (not shown). The observed JA mean surface temperature anomaly is shown in Fig. 10c.

The JUNBLSST-JUNCLSST ensemble June mean surface temperature anomaly contains a large 1°C positive anomaly which is statistically significant near its center in the vicinity of the Great Lakes (Fig.10b). This simulated anomaly is both very weak and shifted to the east compared to that observed, and is directly under the contemporaneous simulated 300 mb geopotential height anomaly (not shown), which was also weaker than that observed. The JUNBLSST-JUNCLSST ensemble JA mean surface temperature anomaly (Fig. 10d) includes a statistically significant 1-2°C positive anomaly which extends across the eastern half of the U.S. and is similar to that observed. The model does not simulate the positive 1 °C anomaly observed over the west coast, because the simulated positive anomalies for both July and August remain eastward of 110°W, unlike those observed (not shown).

5. Impact of soil wetness on the drought and heat wave from June through August

a. Initial soil wetness

The climatological soil wetness used to initialize all the integrations discussed thus far was derived from the proxy observed monthly climatological soil moisture calculated by Willmott et al. (1985). A proxy observed 1988 initial soil wetness is derived from the ECMWF analysis-forecast cycle prognostic soil moisture produced operationally for 1 June 1988. Both ECMWF prognostic soil moisture layers were used, being a surface layer with a maximum capacity of 20 mm of liquid water and a deep soil layer with a maximum capacity of 120 mm of liquid water. The bottom ECMWF soil moisture layer, the deep climatological layer, which is not prognostic but is updated to time-varying climatological values during integration, was not used. Starting in November 1983, the ECMWF forecast model has been integrated in a four-dimensional data-assimilation mode with continuously updated soil moisture, from which a soil moisture time-series is available. Unfortunately, the Willmott et al. climatological soil moisture and the ECMWF 1988 soil moisture cannot be used directly by SiB. The land surface parameterizations (LSPs) used by Willmott et al. and in the ECMWF model are very different from SiB, so the resulting soil moisture fields are different from what would have been calculated by SiB if exposed to the same atmospheric forcings. Sato et al. (1989 b) developed a method to transform soil moisture calculated by other LSPs into the equivalent for SiB. This method was used to transform the Willmott et al. climatological soil moisture. Essentially, the method calculates the time-integral of evaporative demand that a GCM grid area would have to be exposed to dry down from saturation to a specified level. This same time-integral is then applied to a greatly reduced set of SiB energy balance equations to calculate an equivalent SiB soil moisture level. This

procedure is briefly reviewed in the Appendix of this paper which describes the modified version used to transform the ECMWF prognostic soil moisture into SiB compatible soil wetness. Soil wetness is the soil moisture content expressed as a fraction or percent of the maximum liquid water capacity. The SiB model carries three prognostic soil wetnesses, that of the surface layer, the root zone and the gravitational drainage zone. The procedure outlined in the Appendix is used to transform the two combined ECMWF prognostic soil moisture layers into a soil wetness which is used to initialize all three SiB prognostic soil wetness layers. We would like to emphasize that the ECMWF soil moisture described here and the ECMWF LSP parameterization described in the Appendix were in use operationally during 1988, and may be significantly different from those used more recently by ECMWF. We have verified that the SiB compatible transformed soil wetness still retains the interannual variability inherent in the original ECMWF prognostic soil moisture fields, including the dry soil conditions associated with the 1988 U.S. drought (not shown).

b. Impact of initial soil wetness experiments

Three additional COLA GCM 90-day integrations were initialized from the NMC analyses of the observed atmospheric states at 00UTC on 1, 2, and 3 June 1988. Each integration was initialized with 1 June 1988 proxy observed soil wetness (as described above) and forced with global time varying observed SST for 1988 (Reynolds, 1988). The 3 member ensemble of these integrations will be referred to as JUNBLSSTSW, and will be compared to the JUNBLSST ensemble forced with the same SST which was initialized with climatological soil wetness. Finally, an ensemble of three 30-day integrations initialized with 1 June 1988 proxy observed soil

wetness, but with time varying climatological SST specified (JUNCLSSTSW), will be compared to the JUNCLSST ensemble which was initialized with climatological soil wetness and forced with time varying climatological SST. As in all the integrations presented in this paper, the SiB model predicts the soil wetness of the three prognostic layers after initialization.

The impact of the initial soil wetness anomaly on the 1988 U.S. drought and heat wave may be largely local in nature; however, because the initial soil wetness anomaly used in these experiments is global in extent, possible remote effects will also be considered. The impact of the initial soil wetness anomaly on the surface and hydrological processes of the U.S. region will be discussed in sub-section 1. The impact of the initial soil wetness anomaly on the upper level circulation of the northern hemisphere and the possibility of remote influences will be discussed in sub-section 2.

1) IMPACT ON U.S. SURFACE AND HYDROLOGICAL PROCESSES

The 1 June climatological soil wetness used to initialize the JUNBLSST and JUNCLSST ensembles is shown in Fig. 11a. There is a large zonal gradient in soil wetness across the U.S., with very dry values in the west (40% or less of saturated) and very moist values in the east (70-80% of saturated). The initial soil wetness anomaly computed by subtracting the climatological soil wetness from the 1 June 1988 proxy observed soil wetness used to initialize the JUNBLSSTSW and JUNCLSSTSW ensembles is shown in Fig. 11b. The initial anomaly is -20 to -30% (of saturated) across most of the eastern half of the U.S., and is centered over the main precipitation deficit region observed during April and May, 1988. The strong persistence of the soil wetness anomaly can be inferred from Fig. 11c, which shows the 5-day running mean time

series of daily root zone soil wetness averaged over the eastern U.S. (80-100°W, 30-50°N, land grid points only) for the 1 June initial condition member of the JUNCLSST (dotted), JUNBLSST (solid) and JUNBLSSTSW (dashed) integration ensembles. Fig. 11d shows the corresponding evaporation time series.

The area averaged evaporation in the JUNCLSST integration (dotted) declines from values near 5 mm day^{-1} in early June (day 1) when the soil wetness is near 75% of saturated, to values around 2 mm day^{-1} by early August (day 60) when the soil wetness is about 60% of saturated. The area averaged evaporation in the JUNBLSST integration (solid) declines to values around 2 mm day^{-1} by day 40, at which time the soil wetness is about 57% of saturated. The soil wetness (evaporation) in the JUNBLSST integration is lower than that in the JUNCLSST integration from day 10 through day 80 (day 10 through day 70), and the evaporation reaches low levels indicative of plants under evaporative stress (2 mm day^{-1}), 20 days earlier in the JUNBLSST integration. Thus, in this single integration pair, there is a clear negative impact of the observed SST on soil wetness and evaporation in the eastern U.S. during most of June and July (days 10-60), during which time the precipitation was reduced by 1-2 mm day^{-1} in the JUNBLSST integration relative to that in the JUNCLSST integration (not shown). During the last 10 (20) days of these two integrations the soil wetness (evaporation) was increased in the JUNBLSST integration due to increases in vertically averaged moisture flux convergence and precipitation (not shown). This comparison illustrates the importance of including soil moisture feedback even in integrations initialized with the same initial soil wetness.

The areal averaged evaporation in the JUNBLSSTSW integration (dashed) remains at low levels (2 mm day^{-1}) throughout the entire 90 days, during which time the soil wetness remains

at very dry values (about 45%). The plants in the JUNBLSSTSW integration are under continual evaporative stress throughout the entire integration, while those in the JUNBLSST integration do not reach this state until mid-July (day 40). Compared to the JUNBLSST integration, the JUNBLSSTSW integration had much greater vertically averaged moisture flux convergence (2-3 mm day^{-1}) from days 5 through 40, and much greater precipitation (1-2 mm day^{-1}) from days 20 through 45 (not shown). During the second half of the integrations, the vertically averaged moisture flux convergence and precipitation were much more similar. The almost immediate compensation by the moisture flux convergence (by day 5) for the moisture deficit caused by the reduced evaporation in the JUNBLSSTSW integration is in contrast to the results of Oglesby (1990, 1991) in which one month or longer was required for this compensation to occur.

The June mean observed precipitation anomaly is shown in Fig. 12a, and the June mean JUNBLSSTSW-JUNBLSST ensemble precipitation anomaly, evaporation anomaly and surface temperature anomaly are shown in Figs. 12b, 12c and 12d, respectively. The same four anomaly fields, but for the July-August mean (JA), are shown in Figs. 13a-d, respectively. The June mean JUNBLSSTSW-JUNBLSST evaporation anomaly has a significant negative anomaly of 1-3 mm day^{-1} over the eastern half of the U.S. (Fig. 12c), which closely corresponds to the area of significant simulated positive surface temperature anomalies of 1-6°C (Fig. 12d), as well to the area of negative 10-30% initial soil wetness anomalies (Fig. 11b). There is a smaller area of significant simulated negative precipitation anomaly of 0.5-1 mm day^{-1} in this same area (Fig. 12b), which is well situated but small in magnitude compared to the observed June precipitation anomaly (Fig. 12a). The area of significant simulated positive surface temperature anomaly (Fig. 12d) is situated well to the southeast of the observed June surface temperature anomaly (Fig. 10a).

The impact of the proxy observed initial soil wetness in the ensembles done with climatological SST is similar to that in the ensembles done with observed SST. The area of significant positive surface temperature anomaly in the June mean JUNCLSSTSW-JUNCLSST ensemble surface temperature anomaly (not shown) is virtually identical to that depicted in Fig. 12d. The June mean JUNCLSSTSW-JUNCLSST precipitation anomaly (not shown) contains a negative anomaly over the eastern U.S. which is similar to that depicted in Fig. 12b, but of larger magnitude, with anomalies of 1-2 mm day^{-1}. This larger magnitude June simulated precipitation anomaly in the climatological SST ensembles as opposed to the observed SST ensembles may simply be due to the fact that the JUNCLSST ensemble simulated larger June mean precipitation and soil wetness over this region than did the JUNBLSST ensemble (soil wetness shown in Fig 11c). Effectively, larger soil wetness anomalies were maintained in the climatological SST ensemble anomalies (JUNCLSSTSW-JUNCLSST) than in the observed SST ensemble anomalies (JUNBLSSTSW-JUNBLSST).

The JA mean JUNBLSSTSW-JUNBLSST evaporation anomaly has a significant negative anomaly of 0.5-1 mm day^{-1} over the eastern half of the U.S. (Fig. 13c), which closely corresponds to the area of significant simulated positive surface temperature anomaly of 1-3°C (Fig. 13d), as well to the area of negative 10-30% initial soil wetness anomaly (Fig. 11b). The area of significant simulated positive surface temperature anomalies of 2°C is well situated but stronger in magnitude compared to the observed JA anomalies (Fig. 10c). The significant simulated negative precipitation anomalies of 0.5 mm day^{-1} in the midwest, are in close proximity to observed anomalies of similar magnitude, but the significant simulated negative anomalies over the northwestern U.S. and Canada have no counterpart in the observations (Figs. 13b and 13a, respectively).

2) IMPACT ON NORTHERN HEMISPHERE UPPER LEVEL CIRCULATION

The same initial soil wetness anomaly shown for the U.S. region in Fig. 11b is shown for the northern hemisphere in Fig. 14a. In addition to negative drought anomalies in the U.S., positive anomalies of 20-40% (of saturation) cover much of the 60-75°N latitude band, a negative 10-20% anomaly covers Africa from the equator to 10°N, and several anomalies of 10-20% cover parts of Europe and Asia. Fig. 14b shows the June 1988 observed 300 mb geopotential height anomaly, and Figs. 14c and 14d show the JUNBLSSTSW-JUNBLSST ensemble 300 mb geopotential height anomalies for June and JA, respectively. The positive and negative 15 m contour not shown on previous 300 mb geopotential height anomaly figures is included in Figs. 14b-d. The June mean JUNBLSSTSW-JUNBLSST anomalies are in general quite weak and not statistically significant, reaching a magnitude of 30 m over only a few small areas (Fig. 14c). Over the U.S., positive anomalies of 15-30 m are displaced compared to the positive anomaly observed, which reached a magnitude of 150 m over Lake Winnipeg in Canada. The June mean JUNCLSSTSW-JUNCLSST anomalies are similarly weak, but have a more correctly placed (yet not statistically significant) positive 30 m anomaly centered between Lake Winnipeg and the Great Lakes (not shown).

The JUNBLSSTSW-JUNBLSST 300 mb geopotential height anomalies were stronger and more significant in July, when they reached maximum amplitudes (not shown), than in June. The August anomalies are similar but generally weaker and less significant than those in July (not shown). The JA mean JUNBLSSTSW-JUNBLSST anomaly (Fig. 14d) contains a band of 15-30 m positive anomalies across the northern U.S. which resembles the observed anomalies (Fig. 9c), but is for the most part statistically insignificant. Statistically significant JA negative height

anomalies near the large regions of the northern latitudes with positive initial soil wetness anomalies have no counterparts in the observed height anomalies. A large region of small, but statistically significant anomalies over the central and eastern equatorial Pacific appears suggestive of wave interactions with the upstream (westward) extratropics (Fig. 14d). Such interactions could then possibly lead to impacts on the downstream extratropics, including North America.

The relatively small 300 mb geopotential height anomalies simulated over the drought region are in contrast to the results of Branković et al. (1990), who showed positive geopotential height anomalies of 60 m over the Great Lakes region during JJA 1988 in their single integration pair, one of which was forced with prescribed seasonally varying climatological soil moisture.

6. Summary

The 1988 U.S. drought (precipitation deficit) and heat wave were unique in several respects compared to historical droughts over the U.S. The early timing of the drought (AMJ), and the later timing (JJA) and monthly migration of the heat wave, which was largely geographically removed from the precipitation deficit region, stand out in this regard. A series of experiments consisting of COLA GCM integration ensemble pairs was conducted to determine what role forcing by global SST and global soil wetness played in the life cycles of the drought and heat wave.

The April mean APRBLSST-APRCLSST and MAROISST-MARCLSST simulated precipitation and 300 mb geopotential height anomalies are compared to the observed April mean anomalies in order to determine if the observed global SST played a role in forcing the initiation

of the 1988 U.S. drought. The April mean APRBLSST-APRCLSST simulated anomalies bear no resemblance to those observed in the Pacific-North America region and thus are not suggestive of a role for global SST in forcing the drought initiation. The April 1988 eastern equatorial Pacific negative SST anomalies used in the APRBLSST-APRCLSST experiment are weak compared to those found in the new high resolution OI SST analysis of Reynolds and Smith (1994), which are more in accord with buoy data cited by Trenberth and Branstator (1992). Use of the OI SST in the MAROISST-MARCLSST experiment yields April mean simulated precipitation and 300 mb geopotential height anomalies in the Pacific-North America region which are quite similar to those observed during April 1988. A detailed analysis of the MAROISST-MARCLSST results shows that the SST anomalies observed in the eastern equatorial Pacific during April 1988 were capable of forcing the observed wavetrain and precipitation anomalies associated with the beginning of the 1988 U.S. drought. The simulated wavetrain and U.S. drought precipitation anomalies appear closely linked to the strength of the positive precipitation anomalies simulated in the vicinity of 135°W, 12°N . These results agree with the hypothesis of TBA who suggested that the forcing from the eastern equatorial Pacific during AMJ was the primary cause of the drought. Furthermore, they strengthen the TBA hypothesis by showing that this forcing could be responsible for the drought initiation during April. A comparison of the results of the April mean anomalies from the APRBLSST-APRCLSST and MAROISST-MARCLSST experiments verifies the suggestion of Trenberth and Branstator (1992) that it is important to use a SST analysis which accurately depicts the strength of the negative SST anomalies observed in the eastern equatorial Pacific during April, 1988, when attempting to simulate the drought with a GCM.

Results from the last 60 days of APRBLSST-APRCLSST experiment, as well as from the first 30 days of the JUNBLSST-JUNCLSST experiment suggest that the SST related forcing from the eastern equatorial Pacific continued to play a role in contributing to the drought maintenance, during May and June. This is consistent with the SST impact found in previous studies during this period. The June mean JUNBLSSTSW-JUNCLSSTSW ensemble anomalies (not shown), are very similar to the June mean JUNBLSST-JUNCLSST anomalies, which implies that the impact of the observed SST on the drought during June is not dependent on the initial soil wetness used. In all the experiments, this forcing was of similar strength during the months of May and June. This result, in conjunction with the observed occurrence of a particularly large positive anomaly in the 300 mb geopotential height over central North America during June, suggests that the strength of the observed June anomaly is not directly the result of contemporaneous forcing by SST. The strength of the June anomaly may be due to either internal dynamics or additional boundary forcing, such as that of induced soil wetness anomalies over the drought region. An analysis of the time series of soil wetness and evaporation averaged over the eastern half of the U.S. in the JUNCLSST and JUNBLSST ensembles reveals that the observed SST was capable of forcing negative soil wetness and evaporation anomalies over this region during June and July.

Because remote teleconnections are believed to be established in the upper troposphere, the lack of observed upper level anomalies over North America during July and August (JA), implies that it is unlikely that contemporaneous remote forcing by SST or other remote boundary conditions is responsible for climate anomalies observed over North America during JA 1988. The JA results from the JUNBLSST-JUNCLSST experiment are not suggestive of SST forcing

of precipitation anomalies over the U.S. at this time, in agreement with the near normal precipitation observed. The JUNBLSST-JUNCLSST results do suggest that the observed SST, in conjunction with induced soil wetness anomalies, can force positive surface temperature anomalies over the U.S. during June, July and August, however, these anomalies were generally weaker and eastward of those observed.

Determining the impact of observed soil wetness anomalies on the life cycles of the drought and heat wave is greatly complicated by the lack of soil wetness measurements during the drought. The experiments presented here (JUNBLSSTSW-JUNBLSST, JUNCLSSTSW-JUNCLSST) examine the impact of a proxy observed initial soil wetness on the June, July and August simulations. Although only initial soil wetness anomalies are prescribed, the anomalies in the prognostic soil wetness are very persistent and remain throughout the course of the JUNBLSSTSW-JUNBLSST experiment. Furthermore, the anomalies obtained using the proxy observed soil wetness are so large that the evaporation over the eastern half of the U.S. is reduced to values indicative of plants under stress due to lack of moisture in early June, two months earlier than in integrations using climatological initial soil wetness and climatological SST. Without observations it is difficult to judge whether the initial soil wetness anomalies used in these experiments are realistic in magnitude or extent. Field measurements at a site in the middle of the corn belt indicate that the crops were under stress due to lack of moisture by the end of June, at which time the measurements were begun (Kunkel 1990b). Unfortunately, earlier measurements are unavailable.

The results from the JUNBLSSTSW-JUNBLSST and JUNCLSSTSW-JUNCLSST experiments both indicate that the proxy observed initial soil wetness is capable of forcing

negative precipitation anomalies over the drought area in June, and positive surface temperature anomalies over this same region during June, July and August. The simulated June precipitation anomalies are realistic, particularly in the JUNCLSSTSW-JUNCLSST experiment, but the simulated surface temperature anomalies remain located over the drought region during JJA, unlike the observed surface temperature anomalies which migrated from month to month. Thus, a clear impact of initial soil wetness on the drought and heat wave is simulated, and the precipitation anomalies throughout JJA, and the surface temperature anomalies during August, are similar to the observed anomalies. What role the lack of actual observed initial soil wetness has in the inaccuracy of the heat wave simulation is difficult to ascertain. A comparison of the 1 June proxy observed initial soil wetness anomalies used here to the proxy observed May and June soil moisture anomalies used by Atlas et al. (1993, Figs. 3a, 3b) shows that similar magnitude anomalies are used in the mid- and eastern-U.S. drought region, but that the Atlas et al. negative anomalies in the vicinity of 110-115°W, 45-50°N are of greater magnitude than those used here. One can speculate that larger initial soil wetness anomalies in this region might have the effect of shifting the large June surface temperature anomalies simulated in the JUNBLSSTSW-JUNBLSST and JUNCLSSTSW-JUNCLSST experiments towards the northwest, more in accord with the observed June anomalies. However, the Atlas et al. soil moisture forced surface temperature anomalies for their ensemble of three 60-day simulations covering the period from 10 May to 29 July (Atlas et al. Fig. 7) were also displaced to the southeast of those observed.

Given the persistent nature of soil moisture anomalies and the highly variable location of the heat wave from month to month, it may well be that the observed heat wave was largely

modulated by processes related to the internal dynamics of the atmosphere, which would explain both the high variability of the heat wave and the difficulty in simulating this variability with a model. The observed monthly surface temperature anomalies over North America were highly correlated with the observed upper level geopotential height anomalies, as shown by Klein (1990). An examination of the observed monthly anomalies over North America for April through August reveals that the strongest monthly surface temperature anomalies observed (up to 5°C), were located directly under the strongest monthly 300 mb geopotential height anomalies observed (up to 150 m), during June. Mo et al. (1991) showed that much of this large geopotential height anomaly and the wave train of which it was a part, are simulated in the June mean of an NMC MRF integration ensemble initialized from the observed atmospheric state in late May, 1988, even with the use of climatological SST. An examination of the June mean JUNCLSST ensemble departure from the zonal mean of the 300 mb geopotential height reveals a similar result, with a good simulation of much of the observed positive departure over North America (not shown). As in the Mo et. al (1991) simulations, the veracity of this feature was enhanced with the use of observed SST, as seen in the same field from the JUNBLSST ensemble (not shown). Thus it appears likely that the month to month variability of the drought circulation in general, and the strength of the June anomalies in particular, are largely related to internal dynamical processes associated with the atmospheric state, which in turn is subject to conditioning by prior anomalous boundary conditions.

Neither the experiments presented here, nor the results from previous studies of the 1988 U.S. drought suggest a role for anomalous SST or soil wetness in forcing the end of the drought by early July. It is possible that simulations done with the observed soil wetness, were it

available, might suggest such a role. A possible scenario is that moisture convergence feedback induced by the anomalous circulation set up by the soil wetness anomalies could possibly overwhelm the atmospheric moisture deficit associated with the soil wetness anomalies, and thus end the drought. The strong moisture convergence feedback of roughly 2 mm day^{-1} averaged over the eastern half of the U.S. obtained in the JUNBLSSTSW-JUNBLSST experiment, was not enough to offset the atmospheric moisture deficit caused by the 3 mm day^{-1} reduction in evaporation over this region. However, with different soil wetness initial conditions, a different result might be obtained. Another possibility is that the internal dynamic processes apparently responsible for much of the month to month variability of the drought circulation, were also responsible for the end of the drought (precipitation deficit) in early July.

The experiments presented here clearly show important roles for both SST and soil wetness anomalies in forcing the life cycle of the 1988 U.S. drought and heat wave. There is also evidence that the observed SST forcing can interact with the soil wetness forcing. During June the impact of the observed SST on the drought did not depend on the initial soil wetness used, but the impact of the proxy observed initial soil wetness on the drought did depend on the SST used, in that a greater reduction in precipitation was obtained in the integration ensembles done with climatological SST. The way the integrations were conducted, there was no opportunity for the soil wetness to impact the SST, which was prescribed, but the observed SST did impact the prognostic soil wetness in a way compatible with the drought circulation. Given this feedback, and the ability of the proxy observed initial soil wetness to force the drought circulation, the need for an observed or inferred soil moisture data set is clear.

Acknowledgments. The authors would like to thank E. Rasmusson for enlightening discussions during the early stages of this study, P. Dirmeyer for helpful suggestions on the manuscript, R. Reynolds for providing the SST analyses, R. Spencer for providing the MSU oceanic precipitation product, J. Janowiak for his help and advice concerning the CAMS station precipitation and surface temperature data and the GPCC gridded station precipitation data, and T. Palmer and Č. Branković for help in obtaining and interpreting the ECMWF soil wetness analysis.

This research was supported by NASA Grants NAGW-1269 and NAGW-2661, and by NSF Grant ATM-90-19296.

APPENDIX

Transforming ECMWF soil moisture fields into equivalent SiB fields

The transformation method described here is a variation of that developed by Sato et al. (1989 b). Under non-precipitating conditions, the equations governing the drying of a soil column within the ECMWF land surface process (LSP) parameterization can be reduced to:

$$\frac{dS_E}{dt} = -E_E \qquad \textbf{(A.1)}$$

$$E_E = \beta_E E_p \qquad \textbf{(A.2)}$$

$$\beta_E = Max[F_{EV}(W), F_{ES}(W)] \quad \textbf{(A.3)}$$

$$F_{EV}(W) = \frac{W-0.3}{0.6-0.3} \quad , 0<W<1 \quad \textbf{(A.4)}$$

$$F_{ES}(W) = \frac{1}{2}[1-\cos(\frac{\pi W}{2})] \quad \textbf{(A.5)}$$

where S_E is the total soil moisture content in mm, E_E is the evaporation rate in kg $m^{-2}s^{-1}$, E_p is the potential evaporation rate in kg $m^{-2}s^{-1}$, B_E is the soil moisture supply function, $F_{EV}(W)$ is the vegetation controlled evaporation rate function, $F_{ES}(W)$ is the bare soil controlled evaporation rate function, W is the soil wetness = S/S_{max} , where S_{max} = 150 mm in ECMWF model.

In equations (A.1) through (A.5), the supply function limiting the evaporation rate, β_E, is in a form equivalent to the Beta-function of Budyko (1974); (A.4) describes the vegetation-limited rate and (A.5) the bare soil surface rate. In (A.5), the surface soil wetness is assumed to be half that of the entire column due to the effects of surface drying and gravitational drainage. Equivalent formulations can be written for SiB:

$$\frac{dS_S}{dt} = -E_S \quad \textbf{(A.6)}$$

$$E_S = \beta_S E_p \quad \textbf{(A.7)}$$

$$\beta_S = V\, F_{SV}(W) + (1-V)\, F_{SS}(W) \quad \textbf{(A.8)}$$

$$F_{SV}(W) = \frac{\psi - \psi_2}{\psi_1 - \psi_2} \quad , 0<F_{SV}<1 \quad \textbf{(A.9)}$$

$$F_{SS}(W) = h_S \frac{r_{surf0}}{r_{surf}} \qquad \textbf{(A.10)}$$

where the variables in equations (A.6) through (A.10) with 's' subscripts are equivalent to those with 'E' subscripts for equations (A.1) through (A.5) (E for ECMWF, S for SiB); and V is the vegetation cover fraction, ψ is the soil moisture suction in m, $\psi = \psi_S W^{-B}$, ψ_s is the value of ψ at saturation (soil type dependent) in m, B is the soil parameter (soil type dependent) in m, $W = S/S_{max}$, S_{max} is the maximum soil moisture capacity (vegetation type dependent) in mm, h_s is the soil surface relative humidity, r_{surf} is the soil surface resistance (function of W/2) in sm^{-1}, and r_{surf0} = minimum value of r_{surf} in sm^{-1}. Formulations for h_s, r_{surf} and r_{surf0} may be found in Sellers et al. (1986, 1989).

The process of transforming the S_E fields into S_s fields is now fairly straight forward. The link between the Beta-function and SiB soil moisture contents is specified by the time, T, that each grid area is exposed to the same evaporative demand, E_p. Thus, if A.1 and A.6 are rearranged and modified, we have:

$$\int_{S_{max}}^{S_E} \frac{1}{\beta_E}\, dS = -E_p \int_0^T dt = \int_{S_{max}}^{S_S} \frac{1}{\beta_S}\, dS \qquad \textbf{(A.11)}$$

where S_{max} = 150 mm for ECMWF and $S_{max} = (-\psi_S)^{1/B}$ mm for SiB

In (A.11), the values of S_{max} and S_E are known and the formulations for β_E and β_s have been specified. (A.11) can therefore be solved for S_s, the equivalent SiB soil moisture value to S_E, by numerical integration. In practice, a series of numerical integrations are done to create look-up tables of S_s as a function of S_E and vegetation type.

Equation (A.11) can be expected to work acceptably in moist regions. In dry areas, it can be assumed that the soil moisture content has reached a quasi-equilibrium state which is characterized by the value of β_E. Under these conditions, the value of S_s is calculated by matching β_E with a SiB soil moisture suction value, so that $\beta_E = \beta_s$, and

$$S_S = S_{\max} \left[\frac{\psi_S}{\psi}\right]^{\frac{1}{\beta}} \qquad \textbf{(A.12)}$$

Where β is determined from the solution of (A.3) and (A.8). Again off-line calculations are used to generate look-up tables. The minimum value of S_s given by (A.11) and (A.12) is used for the SiB initialization.

In the current study, the SiB vegetation was simplified for the soil moisture initialization. All the non-forested regions (grasslands, pasture, deserts, agriculture) were assigned $F_{sv}(W)$ and $F_{ss}(W)$ properties associated with agriculture; this produced smoother fields of S_s over the mid-continental areas.

REFERENCES

Alpert, J. C., M. Kanamitsu, P. M. Caplan, J. G. Sela, G. H. White and E. Kalnay, 1988: Mountain induced gravity wave drag parameterization in the NMC medium-range forecast model. Proceedings of the Eight AMS Conference on Numerical Weather Prediction, 22-26 February, 1988, AMS, Boston, MA, 726-733.

Anthes, R. A., 1977: A cumulus parameterization scheme utilizing a one-dimensional cloud model. *Mon. Wea Rev.*, **105,** 270-300.

Atlas, R., N. Wolfson and J. Terry, 1993: The effect of SST and soil moisture anomalies on GLA Model Simulations of the 1988 U.S. Summer Drought. *J. Climate,* ***6,*** 2034-2048.

Branković, Č., T. N. Palmer and P. Viterbo, 1990: Diagnostic and model sensitivity study of the 1988 U.S. drought. **Proc. Workshop on 1988 U.S. Drought,** 30 April - 2 May, 1990, Dept. of Meteorology, University of Maryland, College Park, MD 20742, 110-128.

Budyko, M. I., 1974: **Climate and Life.** Academic Press, 508 pp.

Fennessy, M. J., J. L. Kinter III, B. Kirtman, L. Marx, S. Nigam, E. Schneider, J. Shukla, D. Straus, A. Vernekar, Y. Xue, and J. Zhou, 1994: The simulated Indian monsoon: A GCM sensitivity study. *J. Climate,* **7,** 33-43.

Fennessy, M. J., L. Marx, J. L. Kinter III and J. Shukla, 1990: The influence of global sea surface temperature on the 1988 U.S. drought: A comparison of simulations with two general circulation models. **Proc. Workshop on 1988 U.S. Drought,** 30 April - 2 May, 1990, Dept. of Meteorology, University of Maryland, College Park, MD 20742, 173-194.

Harshvardhan, R. Davies, D. A. Randall and T. G. Corsetti, 1987: A fast radiation parameterization for general circulation models. *J. Geophys. Res.,* **92,** 1009-1016.

Heim, R. R., 1990: The 1988 drought in the United States: Overview and historical perspective. **Proc. Workshop on 1988 U.S. Drought,** 30 April - 2 May, 1990, Dept. of Meteorology, University of Maryland, College Park, MD 20742, 14-48.

Hou, Y.-T., 1990: Cloud-Radiation-Dynamics Interaction. Ph.D. Thesis, Dept. of Meteorology, University of Maryland, College Park, MD 20742.

Janowiak, J. E., 1988: The global climate for March-May 1988: The end of the 1986-1987 Pacific warm episode and the onset of widespread drought in the United States. *J. Climate,* **1,** 1019-1040.

Janowiak, J. E. and P. A. Arkin, 1991: Rainfall variations in the tropics during 1986-1989, as estimated from observations of cloud-top temperature. *J. Geophys. Res.*, **96,** 3359-3373.

Kinter III, J. L., J. Shukla, L. Marx and E. K. Schneider, 1988: A simulation of the winter and summer circulations with the NMC global spectral model. *J. Atmos. Sci.*, **45,** 2486-2522.

Klein, W. H., 1990: The anomalous weather of the 1988 drought relative to the observed 700 mb circulation. **Proc. Workshop on 1988 U.S. Drought,** 30 April - 2 May, 1990, Dept. of Meteorology, University of Maryland, College Park, MD 20742, 49-74.

Kousky, V. E., 1990: Atmospheric circulation features prior to and during the 1988 drought. **Proc. Workshop on 1988 U.S. Drought,** 30 April - 2 May, 1990, Dept. of Meteorology, University of Maryland, College Park, MD 20742, 75-82.

Kunkel, K. E., 1990a: Operational soil moisture estimation for the midwestern United States. *J. Appl. Met.,* **29,** 1158-1166.

Kunkel, K. E., 1990b: Measurements and estimates of evaporation in the midwestern United States during the 1988 drought. **Proc. Workshop on 1988 U.S. Drought,** 30 April - 2 May, 1990, Dept. of Meteorology, University of Maryland, College Park, MD 20742, 83-95.

Kuo, H. L., 1965: On the formation and intensification of tropical cyclones through latent heat release by cumulus convection. *J. Atmos. Sci.*, **22,** 40-63.

Lacis, A. A. and J. E. Hansen, 1974: A parameterization for the absorption of solar radiation in the earth's atmosphere. *J. Atmos. Sci.*, **31,** 118-133.

Lau, K. M. and L. Peng, 1990: Dynamics of summertime teleconnection over North America. **Proc. Workshop on 1988 U.S. Drought,** 30 April - 2 May, 1990, Dept. of Meteorology, University of Maryland, College Park, MD 20742, 96-109.

Lau, K. M. and L. Peng, 1992: Dynamics of atmospheric teleconnections during the northern summer. *J. Climate,* **5,** 140-158.

Liston, G. E., Y. C. Sud and G. K. Walker, 1993: Design of a global soil moisture initialization procedure for the Simple Biosphere Model. NASA Tech. Memo. 104590, 130 pp.

Lyon, B., 1991: An observational study of persistent temperature anomalies over the North American region. Ph.D Thesis, Mass. Inst. of Tech., 172 pp.

Mellor, G. L. and T. Yamada, 1982: Development of a turbulence closure model for geophysical fluid problems. *Rev. Geophys. Space Phys.,* **20,** 851-875.

Miyakoda, K. and J. Sirutis, 1977: Comparative integrations of global spectral models with various parameterized processes of subgrid scale vertical transports. *Beitr. Phys. Atmos.*, **50,** 445-447.

Mo, K., J. R. Zimmerman, E. Kalnay and M. Kanamitsu, 1990: A GCM study of the 1988 U.S. drought. **Proc. Workshop on 1988 U.S. Drought,** 30 April - 2 May, 1990, Dept. of Meteorology, University of Maryland, College Park, MD 20742, 163-169.

Mo, K., J. R. Zimmerman, E. Kalnay and M. Kanamitsu, 1991: A GCM study of the 1988 United States drought. *Mon. Wea Rev., **119,*** 1512-1532.

Namias, J., 1991: Spring and summer drought over the contiguous U.S. - Causes and Prediction. *J. Climate,* **4,** 54-65.

Oglesby, R. J., 1990: Springtime soil moisture, natural climatic variability, and North American summertime drought. Proc. Workshop on 1988 U.S. Drought, 30 April - 2 May, 1990, Dept. of Meteorology, University of Maryland, College Park, MD 20742, 129-141.

Oglesby, R. J., 1991: Springtime soil moisture, natural climatic variability, and North American drought as simulated by the NCAR Community Climate Model 1. *J. Climate,* **4,** 890-897.

Palmer, T. N., 1987: Modelling low frequency variability of the atmosphere. **Atmospheric and Oceanic Variability.** Ed. H. Cattle. Royal Met. Soc., 75-103.

Palmer, T. N. and Č. Branković, 1989: The 1988 US drought linked to anomalous sea surface temperature. *Nature*, 338, 54-57.

Philips, N. A., 1957: A coordinate system having some special advantages for numerical forecasting. *J. Meteor.,* **14,** 184-185.

Plumb, R. A., 1985: On the three-dimensional propagation of stationary waves. *J. Atmos. Sci.,* **42,** 217-229.

Reynolds, R. W., 1988: A real-time global sea surface temperature analysis. *J. Climate,* **1,** 75-86.

Reynolds, R. W., and L. Roberts, 1987: A global sea surface temperature climatology from in situ, satellite and ice data. *Trop. Ocean-Atmos. Newslett.,* **37,** 15-17.

Reynolds, R. W. and T. M. Smith, 1994: Improved global sea surface temperature analyses using optimum interpolation. To appear in *J. Climate,* **7.**

Ropelewski, C. F., 1988: The global climate for June-August 1988: A swing to positive phase of the Southern Oscillation, drought in the United States and abundant rain in monsoon areas. *J. Climate,* **1,** 1153-1174.

Ropelewski, C. F., J. E. Janowiak and M. F. Halpert, 1985: The analysis and display of real time surface climate data. *Mon. Wea. Rev.*, **113,** 1101-1107.

Sardeshmukh, P. D. and B. J. Hoskins, 1988: On the generation of global rotational flow by steady idealized tropical divergence. *J. Atmos. Sci.*, **45**, 1228-1251.

Sato, N., P. J. Sellers, D. A. Randall, E. K. Schneider, J. Shukla, J. L. Kinter III, Y-T. Hou and E. Albertazzi, 1989a: Effects of implementing the Simple Biosphere Model in a general circulation model. *J. Atmos. Sci.*, **46,** 2757-2782.

Sato, N., P.J. Sellers, D. A. Randall, E. K. Schneider, J. Shukla, J. Kinter, Y-T. Hou and E. R. Albertazzi, 1989b: Implementing the Simple Biosphere Model (SiB) in a GCM: Methodology and Results. NASA Contractor Report, CR-185509, NASA HQ, Washington, D.C., USA, 76 pp.

Sela, J. G., 1980: Spectral modeling at the National Meteorological Center. *Mon. Wea. Rev.*, **108**, 1279-1292.

Sellers, P. J., 1990: Specifying surface boundary conditions for drought studies. **Proc. Workshop on 1988 U.S. Drought,** 30 April - 2 May, 1990, Dept. of Meteorology, University of Maryland, College Park, MD 20742, 170-172.

Sellers, P. J., Y. Mintz, Y. C. Sud and A. Dalcher, 1986: A simple biosphere model (SiB) for use within general circulation models. *J. Atmos. Sci.* **43**, 505-531.

Sellers, P. J., J. W. Shuttleworth, J. L. Dorman, A. Dalcher and J. M. Roberts, 1989: Calibrating the Simple Biosphere Model (SiB) for Amazonian Topical Forest using Field and Remote Sensing Data: Part I, Average Calibration with Field Data. *J. Appl. Meteor.*, **28,** 727-759.

Slingo, J. M., 1987: The development and verification of a cloud prediction scheme for the ECMWF model. *Q. J. Roy. Meteor. Soc.*, **103,** 29-43.

Spencer, R., 1993: Global oceanic precipitation from the MSU during 1979-1991, and comparisons to other climatologies. *J. Climate,* **6,** 1301-1326.

Sud, Y. C., K. M. Lau and G. K. Walker, 1990: Model simulation of atmospheric circulation and rainfall for June and July 1988. **Proc. Workshop on 1988 U.S. Drought,** 30 April - 2 May, 1990, Dept. of Meteorology, University of Maryland, College Park, MD 20742, 142-162.

Tugi, M., A. Kitoh and T. Tokioka, 1990: Influence of SSTA on the 1988 summer circulation simulated by MRI-GCM. **Proc. Workshop on 1988 U.S. Drought,** 30 April - 2 May, 1990, Dept. of Meteorology, University of Maryland, College Park, MD 20742, 195-209.

Tiedtke, M., 1984: The effect of penetrative cumulus convection on the large-scale flow in a general circulation model. *Beitr. Phys. Atmos.*, **57**, 216-239.

Trenberth, K. E., 1990: Diagnostic analysis of the 1988 North American drought. **Proc. Workshop on 1988 U.S. Drought,** 30 April - 2 May, 1990, Dept. of Meteorology, University of Maryland, College Park, MD 20742, 1-13.

Trenberth, K. E. and G. W. Branstator, 1992: Issues in establishing causes of the 1988 drought over North America. *J. Climate,* **5,** 159-172.

Trenberth, K. E., G. W. Branstator and P. A. Arkin, 1988: Origins of the 1988 North American Drought. *Science*, **242**, 1640-1645.

Vernekar, A. , B. Kirtman, J. Zhou and D. Dewitt, 1992: Orographic gravity-wave drag effects on medium-range forecasts with a general circulation model. **Physical Processes in Atmospheric Models,** Editors: D. R. Sikka and S. S. Singh, Wiley Eastern Limited, New Delhi, 295-307.

Willmott, C. J., C. M. Rowe and Y. Mintz, 1985: Climatology of the terrestrial seasonal water cycle. *J. Climatol.,* **5,** 589-606.

Xue, Y., P. J. Sellers, J. L. Kinter and J. Shukla, 1991: A simplified biosphere model for global climate studies. *J. Climate,* **4,** 345-364.

Figure Legends

Fig. 1. Blended sea surface temperature anomaly (Reynolds, 1988) for (a) March 1988, (b) April 1988 and (c) May 1988. Contours are ± 0.5, 1, 2, 3, 4 °C. Dashed contours are negative.

Fig. 2. Precipitation anomalies for (a) April mean of observations and (b) 1-30 day mean of APRBLSST - APRCLSST ensemble. Contours are ± 1, 2, 4, 8 mm day^{-1}. Geopotential height anomalies at 300 mb for (c) April mean of observations and (d) 1-30 day mean of APRBLSST - APRCLSST ensemble. Contour interval is 30 meters. Dashed contours are negative. In (b) and (d), areas where anomaly significant at 95% level shaded.

Fig. 3. OI sea surface temperature anomaly (Reynolds and Smith, 1994) for (a) March 1988, (b) April 1988 and (c) May 1988. Contours are ± 0.5, 1, 2, 3, 4 °C. Dashed contours are negative.

Fig. 4. OI sea surface temperature anomaly (Reynolds and Smith, 1994) for week centered on (a) 13 March 1988, (b) 20 March 1988 and (c) 27 March 1988. Contours are ± 0.5, 1, 2, 3 °C. Dashed contours are negative.

Fig. 5. Mean of days 31-60 of precipitation anomalies for MARBLSST - MARCLSST (a) ensemble, (b) 1 June 1988, (c) 2 June 1988 and (d) 3 June 1988. Contour are ± 1, 2, 4, 8 mm day^{-1}. Dashed contours are negative. In (a) areas where anomaly significant at 95% level shaded.

Fig. 6. Mean of days 31-60 of geopotential height anomalies at 300 mb for MARBLSST - MARCLSST (a) ensemble, (b) 1 June 1988, (c) 2 June 1988 and (d) 3 June 1988. Contour

interval is 30 meters. Dashed contours are negative. In (a) areas where anomaly significant at 95% level shaded.

Fig. 7. Blended sea surface temperature anomaly (Reynolds, 1988) for (a) June 1988, (b) July 1988 and (c) August 1988. Contours are ± 0.5, 1, 2, 3, 4 °C. Dashed contours are negative.

Fig. 8. Precipitation anomalies for (a) May-June mean of observations and (b) 31-90 day mean of APRBLSST - APRCLSST ensemble. Contours are ± 1, 2, 4, 8 mm day^{-1}. Geopotential height anomalies at 300 mb for (c) May-June mean of observations and (d) 31-90 day mean of APRBLSST - APRCLSST ensemble. Contour interval is 30 meters. Dashed contours are negative. In (b) and (d), areas where anomaly significant at 95% level shaded.

Fig. 9. Precipitation anomalies for (a) July-August mean of observations and (b) 31-90 day mean of JUNBLSST - JUNCLSST ensemble. Contours are ± 1, 2, 4, 8 mm day^{-1}. Geopotential height anomalies at 300 mb for (c) July-August mean of observations and (d) 31-90 day mean of JUNBLSST - JUNCLSST ensemble. Contour interval is 30 meters. Dashed contours are negative. In (b) and (d), areas where anomaly significant at 95% level shaded.

Fig. 10. Surface temperature anomalies for (a) June mean of observations, (b) 1-30 day mean of JUNBLSST - JUNCLSST ensemble, (c) July-August mean of observations and (d) 31-90 day mean of JUNBLSST - JUNCLSST ensemble. Contours are ± 0.5, 1, 2, 3, 4, 5 °C. Dashed contours are negative. In (b) and (d), areas where anomaly significant at 95% level shaded.

Fig. 11. (a) Initial climatological soil wetness for 1 June. Contour interval is 10 %. (b) Initial soil wetness anomaly for 1 June 1988. Contour interval is 10 %. (c) Five-day running mean eastern U. S. root zone soil wetness (%) for JUNCLSST (dotted), JUNBLSST (solid) and JUNBLSSTSW (dashed). (d) as in (c), but for evaporation (mm day^{-1}).

Fig. 12. (a) June mean observed precipitation anomaly. (b-d) Mean of days 1-30 of JUNBLSSTSW - JUNBLSST ensemble for (b) precipitation, (c) evaporation and (d) surface temperature. Contours in (a), (b) and (c) are ± 0.5, 1, 2, 3, 4 mm day^{-1} . Contours in (d) are ± 0.5, 1, 2, 3, 4, 5, 6 °C. Dashed contours are negative. In (b), (c) and (d), areas where anomaly significant at 95% level shaded.

Fig. 13. (a) July-August mean observed precipitation anomaly. (b-d) Mean of days 31-90 of JUNBLSSTSW - JUNBLSST ensemble for (b) precipitation, (c) evaporation and (d) surface temperature. Contours in (a), (b) and (c) are ± 0.5, 1, 2, 3, 4 mm day^{-1} . Contours in (d) are ± 0.5, 1, 2, 3, 4, 5, 6 °C. Dashed contours are negative. In (b), (c) and (d), areas where anomaly significant at 95% level shaded.

Fig. 14. (a) Initial soil wetness anomaly for 1 June 1988. Contour interval is 10 %. (b-d) Geopotential height at 300 mb for (b) June mean of observations, (c) Mean of days 1-30 of JUNBLSSTSW - JUNBLSST ensemble and (d) Mean of days 31-90 of JUNBLSSTSW - JUNBLSST ensemble. Countour interval in (a) is 10 %. Contours in (b), (c) and (d) are ± 15, 30, 60, 90, 120, 150, 180 meters. Dashed contours are negative. In (c) and (d), areas where anomaly significant at 95% level shaded.

Figure 1

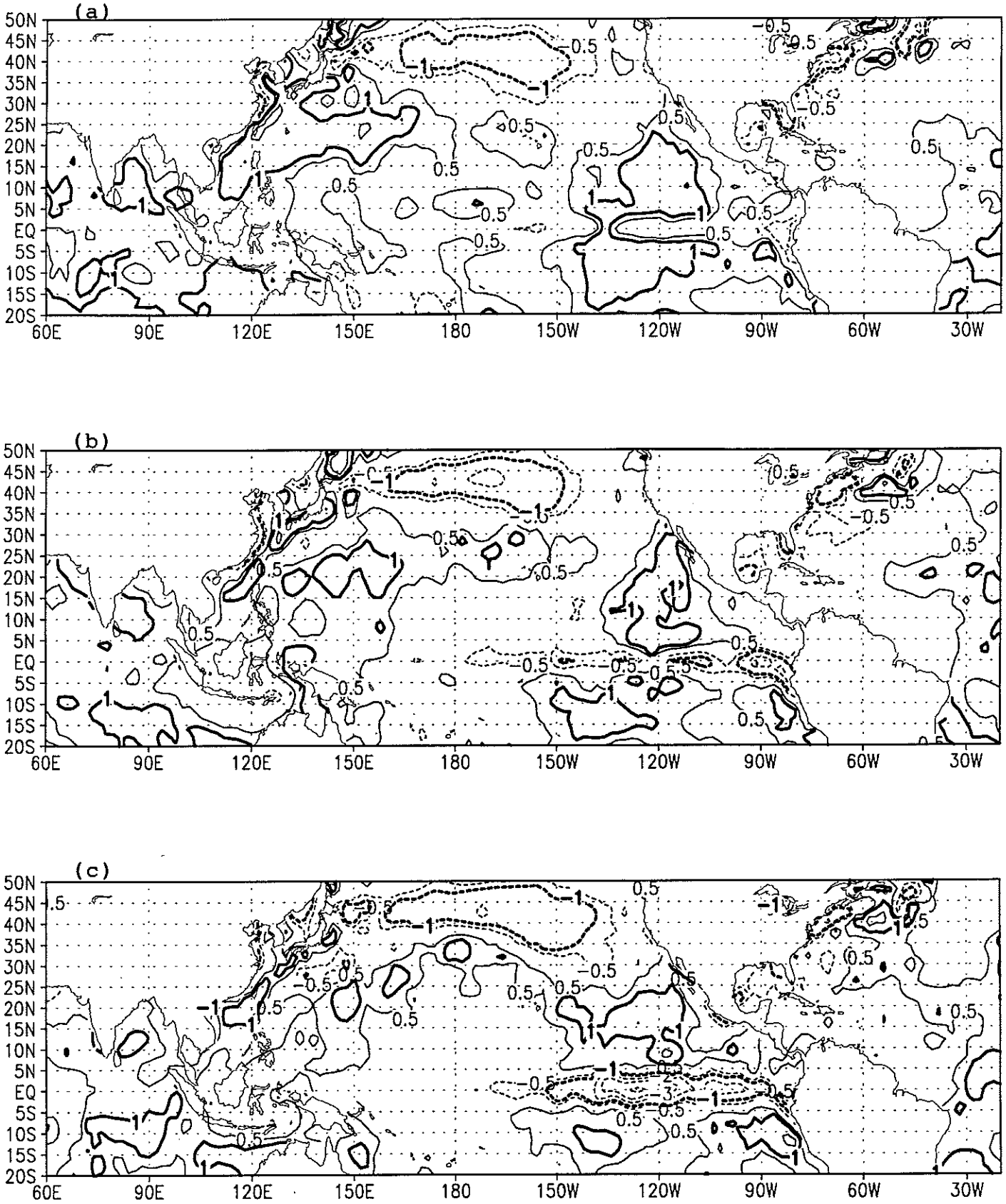
(a)
(b)
(c)
50N
45N
40N
35N
30N
25N
20N
15N
10N
5N
EQ
5S
10S
15S
20S
60E
90E
120E
150E
180
150W
120W
90W
60W
30W

Figure 2

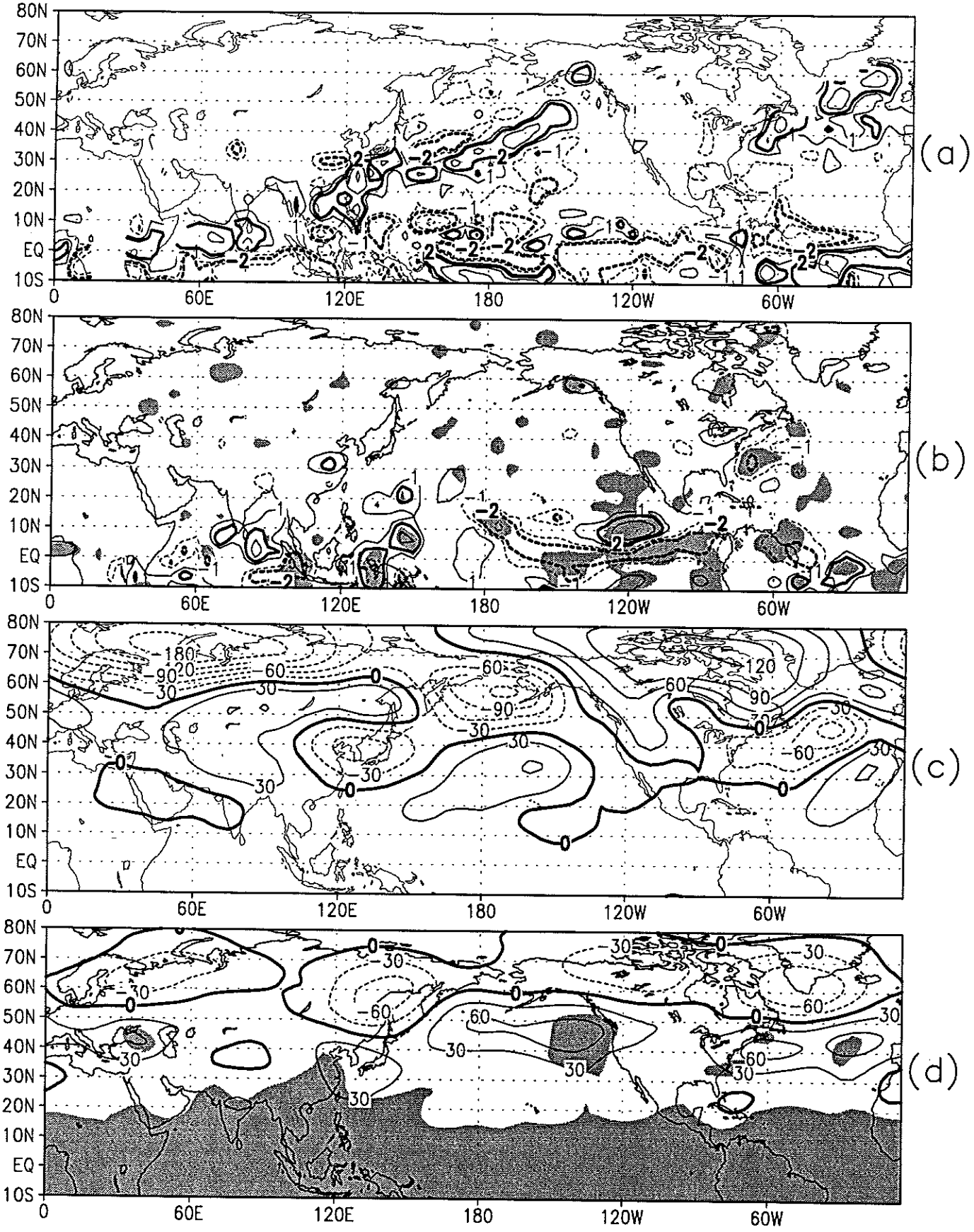
80N
70N
60N
50N
40N
30N
20N
10N
EQ
10S
0
60E
120E
180
120W
60W
(a)
(b)
(c)
(d)

Figure 3

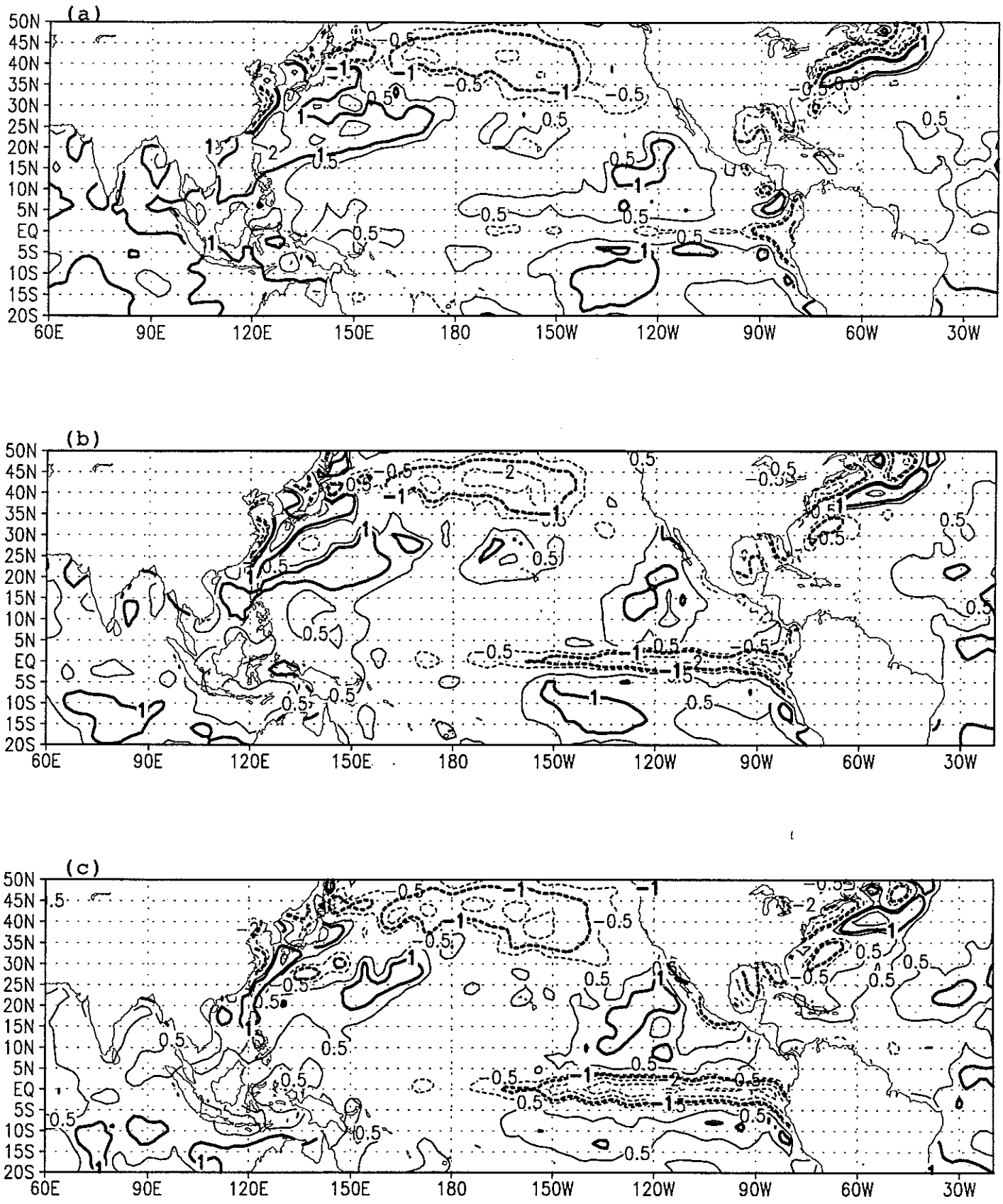
(a)
(b)
(c)
50N
45N
40N
35N
30N
25N
20N
15N
10N
5N
EQ
5S
10S
15S
20S
60E
90E
120E
150E
180
150W
120W
90W
60W
30W

Figure 4

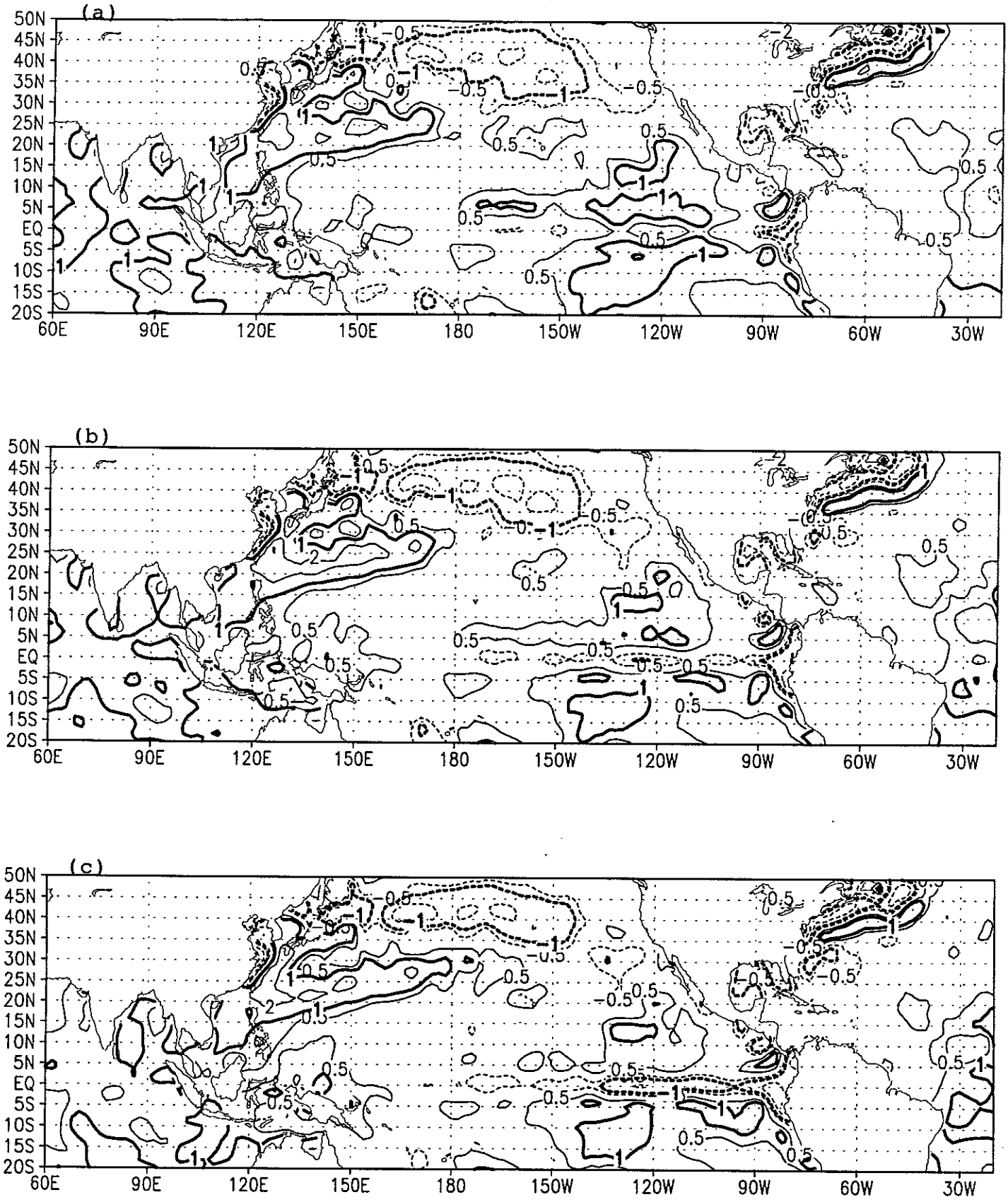
(a)
(b)
(c)
50N
45N
40N
35N
30N
25N
20N
15N
10N
5N
EQ
5S
10S
15S
20S
60E
90E
120E
150E
180
150W
120W
90W
60W
30W

Figure 5

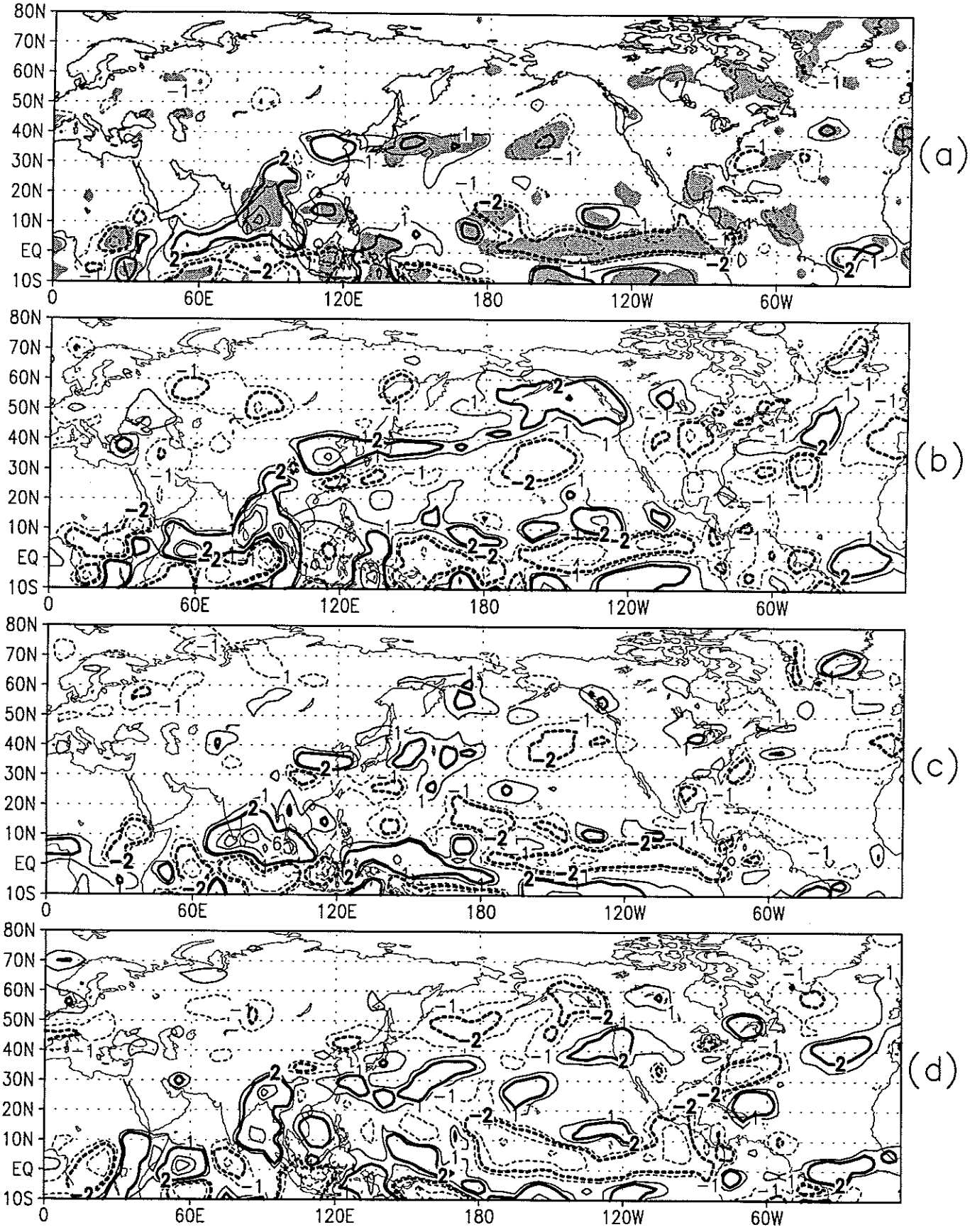
80N
70N
60N
50N
40N
30N
20N
10N
EQ
10S
0
60E
120E
180
120W
60W
(a)
(b)
(c)
(d)

Figure 6

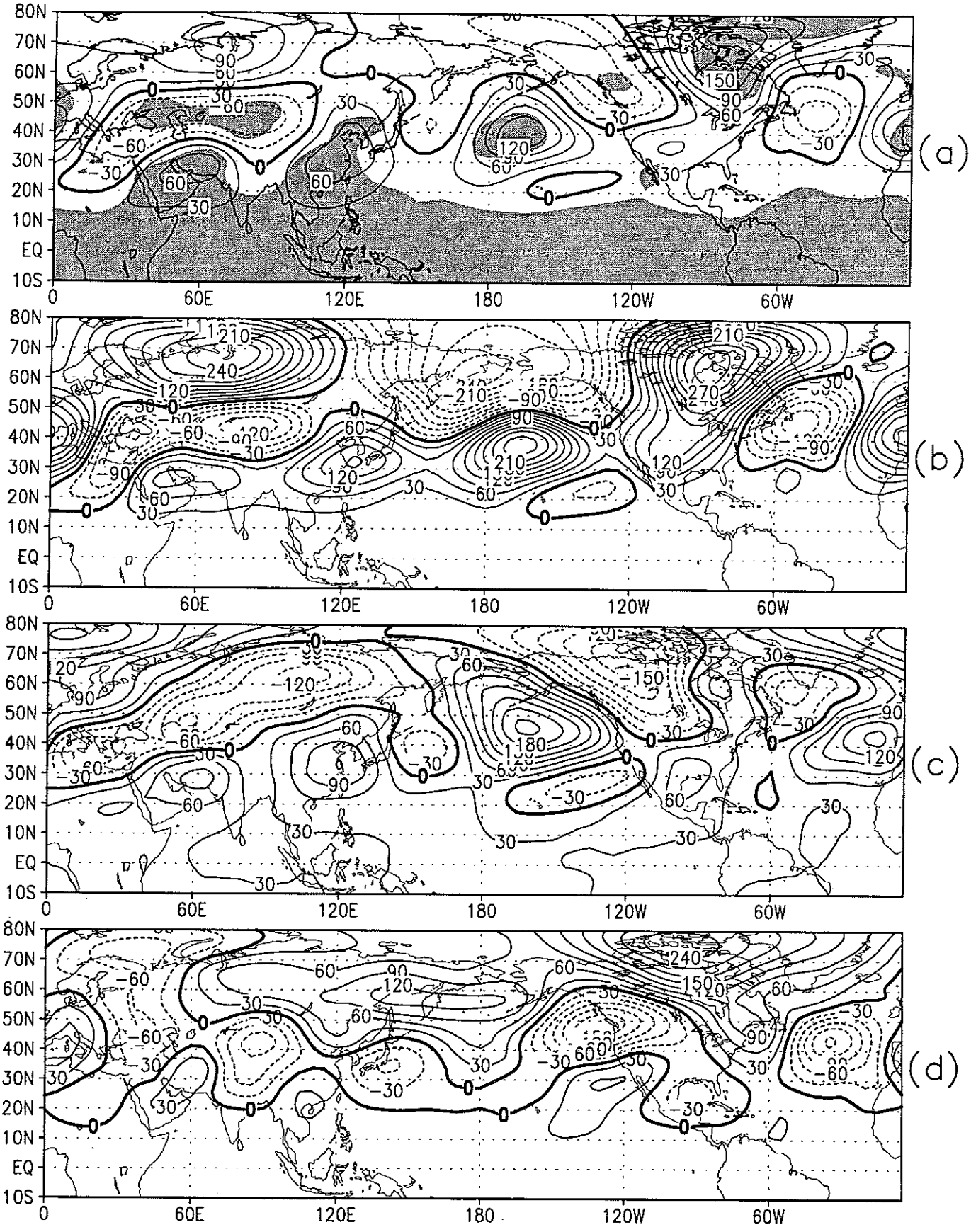
80N
70N
60N
50N
40N
30N
20N
10N
EQ
10S
0
60E
120E
180
120W
60W
(a)
(b)
(c)
(d)

Figure 7

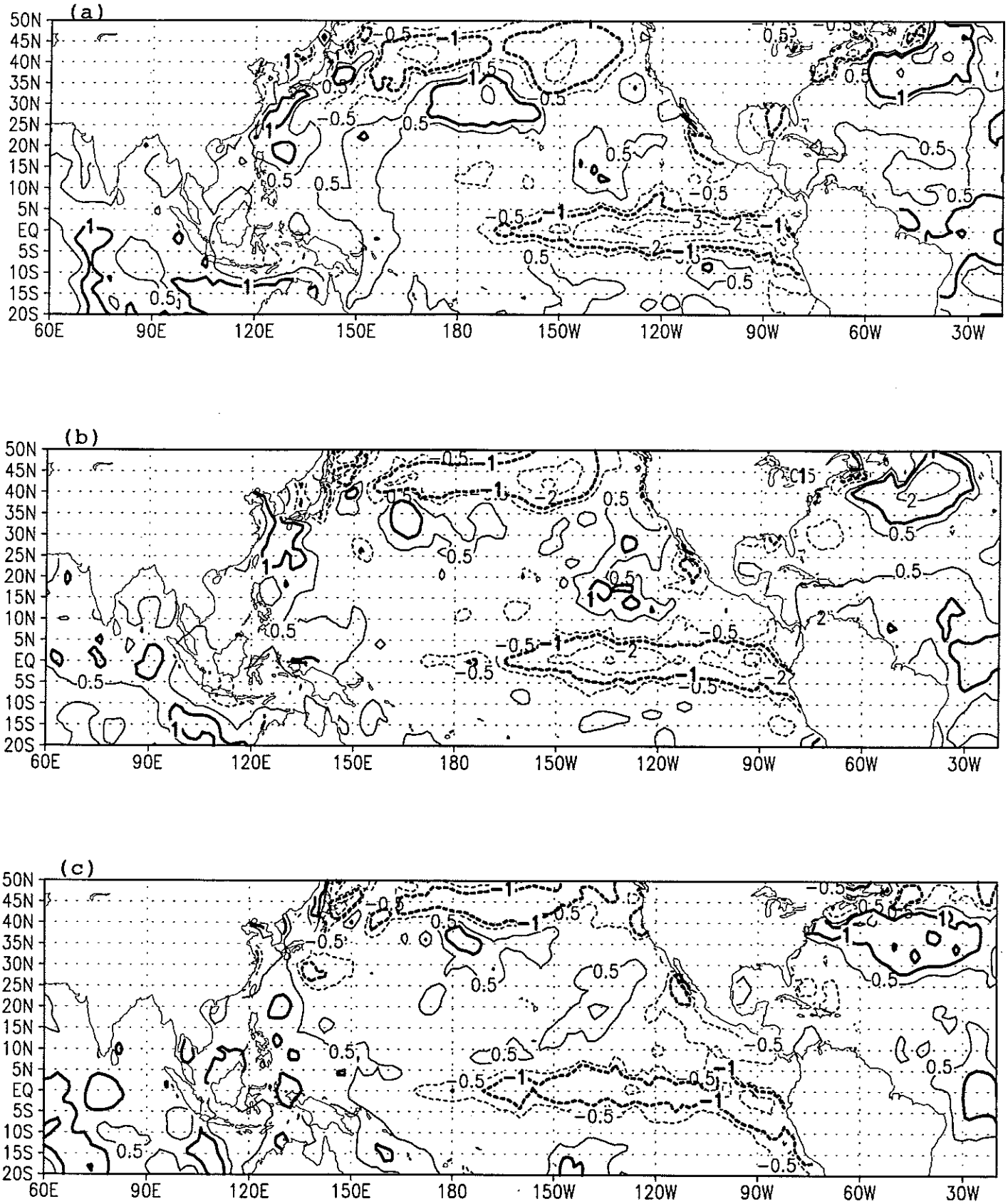
(a)
(b)
(c)
50N
45N
40N
35N
30N
25N
20N
15N
10N
5N
EQ
5S
10S
15S
20S
60E
90E
120E
150E
180
150W
120W
90W
60W
30W

Figure 8

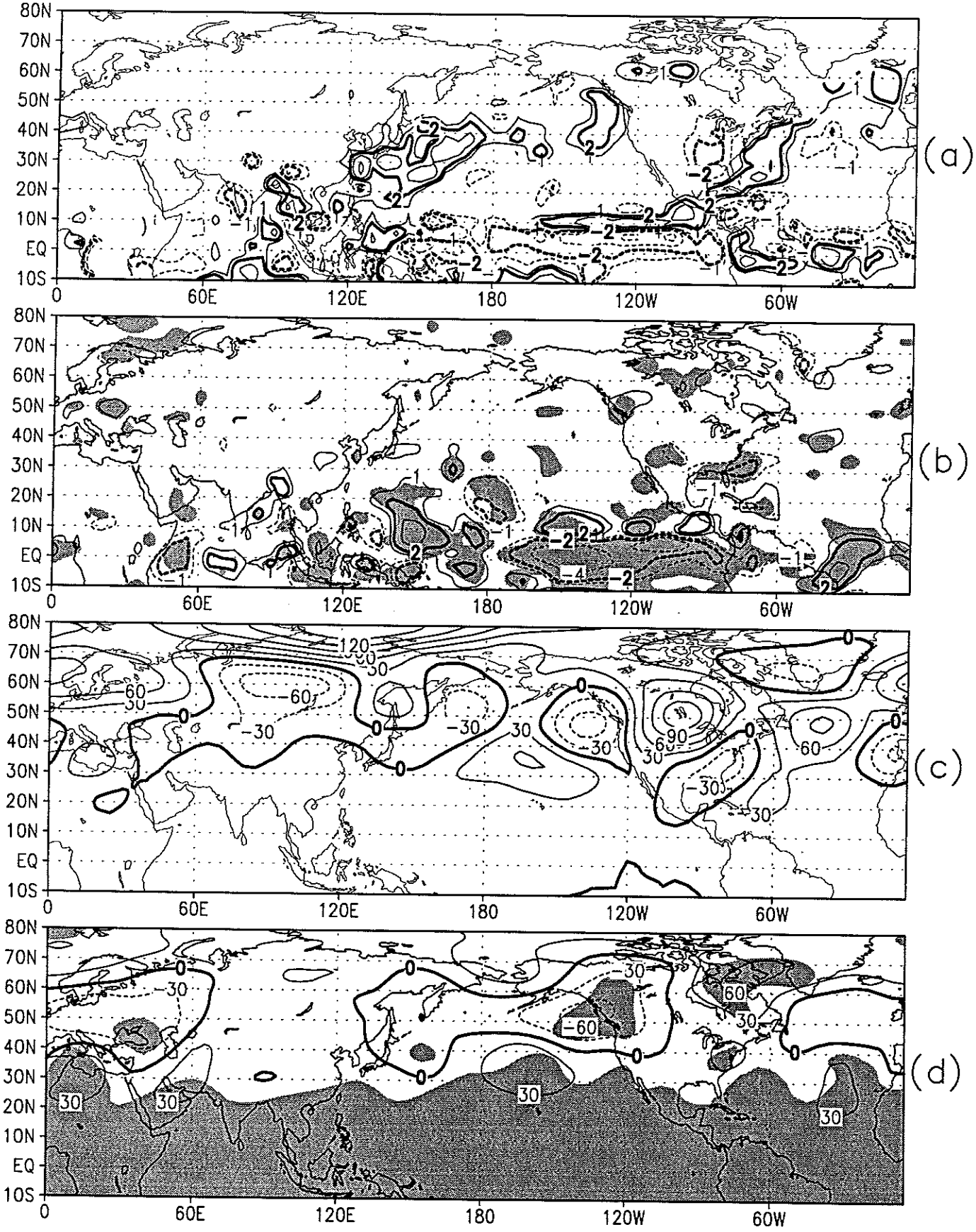
80N
70N
60N
50N
40N
30N
20N
10N
EQ
10S
0
60E
120E
180
120W
60W
(a)
(b)
(c)
(d)

Figure 9

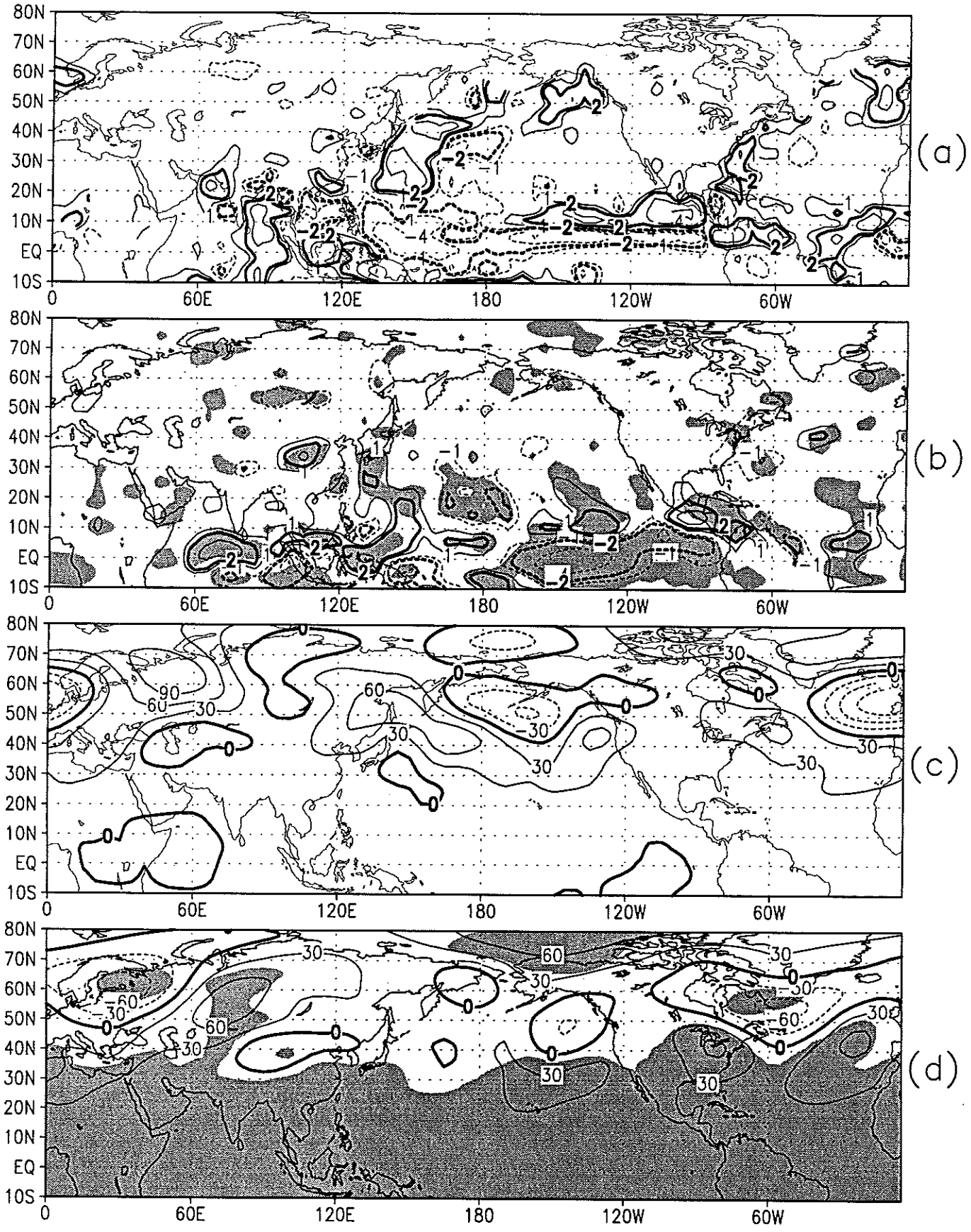
80N
70N
60N
50N
40N
30N
20N
10N
EQ
10S
0
60E
120E
180
120W
60W
(a)
(b)
(c)
(d)

Figure 10

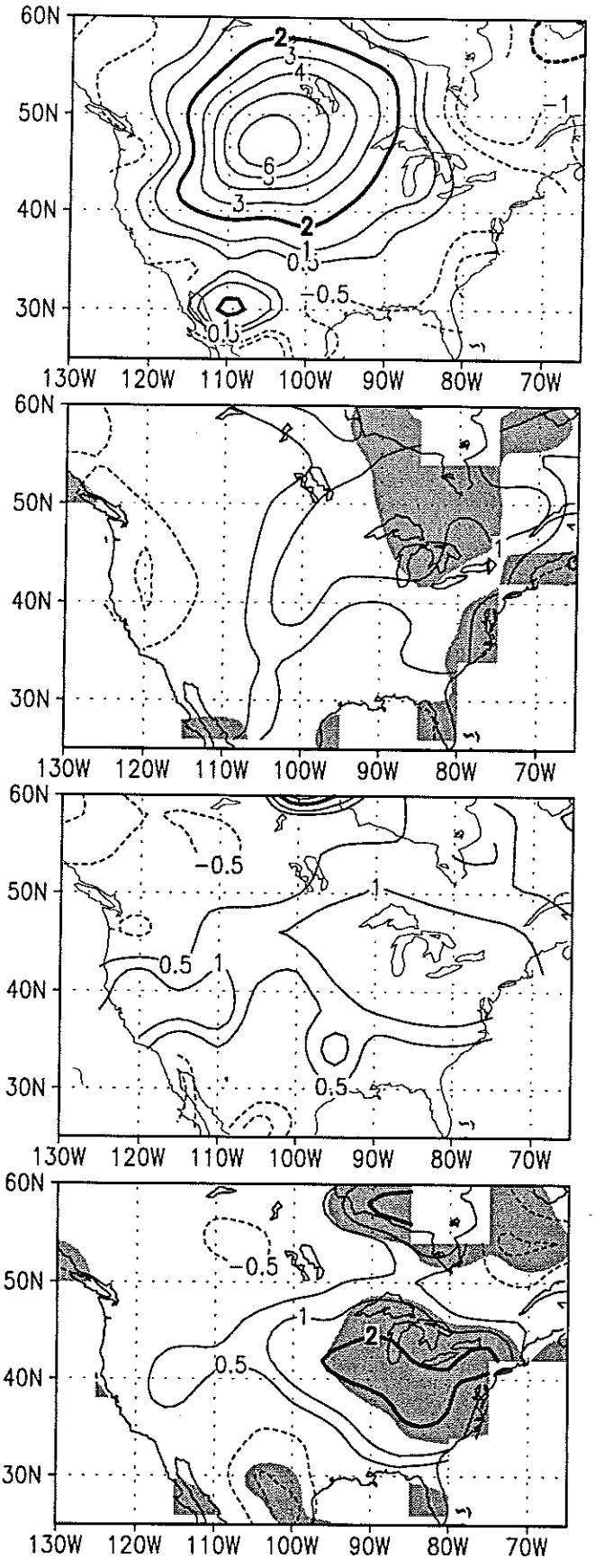
60N
50N
40N
30N
130W 120W 110W 100W 90W 80W 70W
2
3
4
6
3
2
1
0.5
-0.5
-0.1
-1
(a)
1
(b)
-0.5
0.5
1
0.5
(c)
-0.5
1
2
0.5
(d)

Figure 11

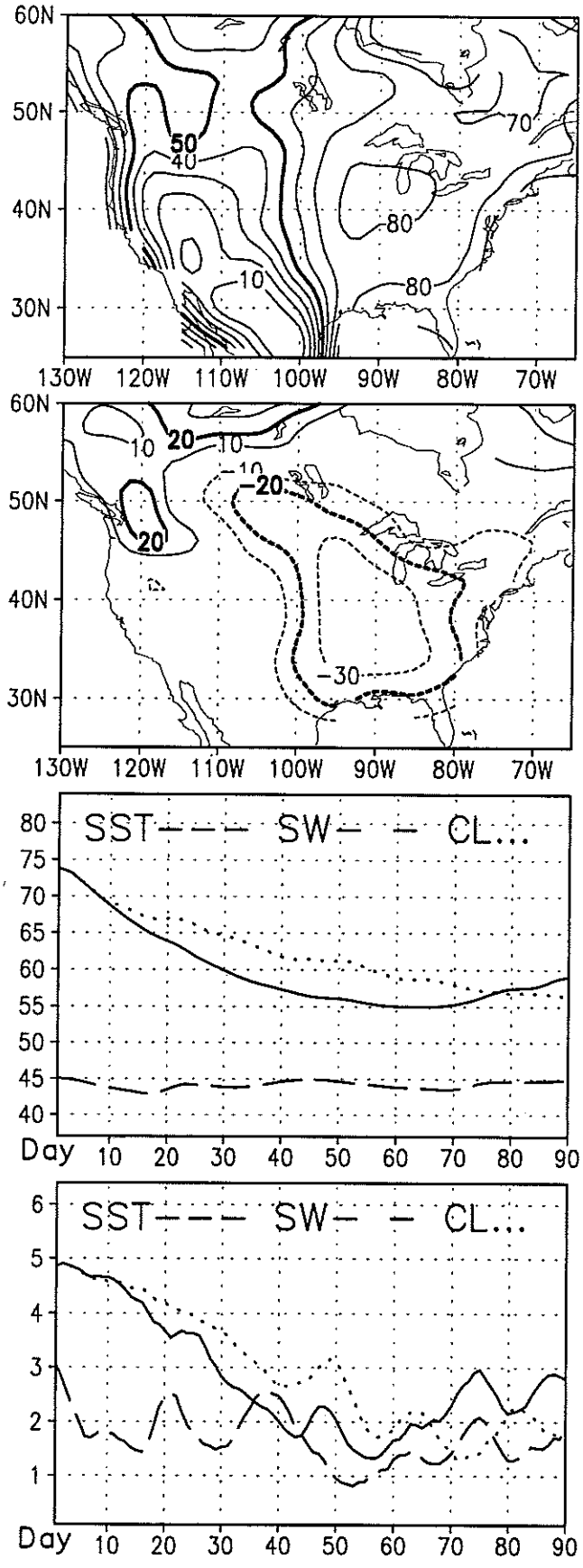
60N
50N
40N
30N
130W 120W 110W 100W 90W 80W 70W
50
40
10
70
80
80
(a)
60N
50N
40N
30N
130W 120W 110W 100W 90W 80W 70W
10
20
10
10
20
20
30
(b)
SST SW CL
80
75
70
65
60
55
50
45
40
Day 10 20 30 40 50 60 70 80 90
(c)
SST SW CL
6
5
4
3
2
1
Day 10 20 30 40 50 60 70 80 90
(d)

Figure 12

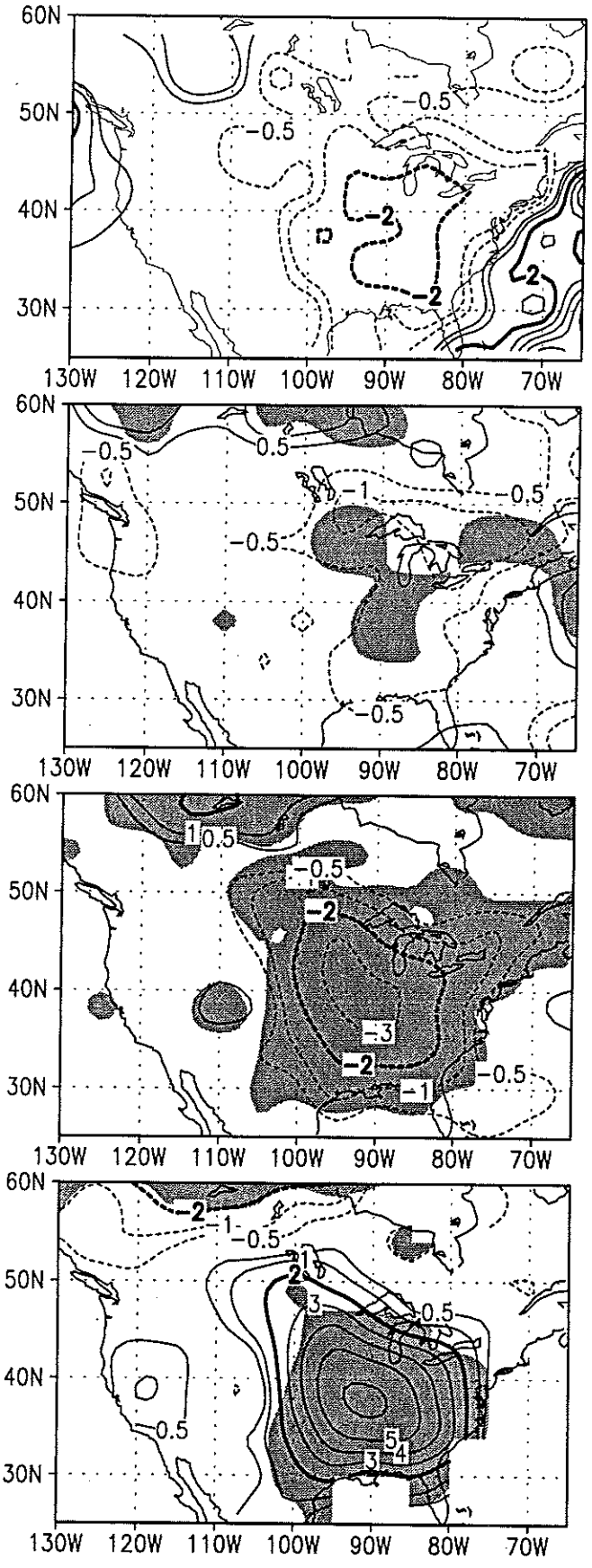

Figure 13

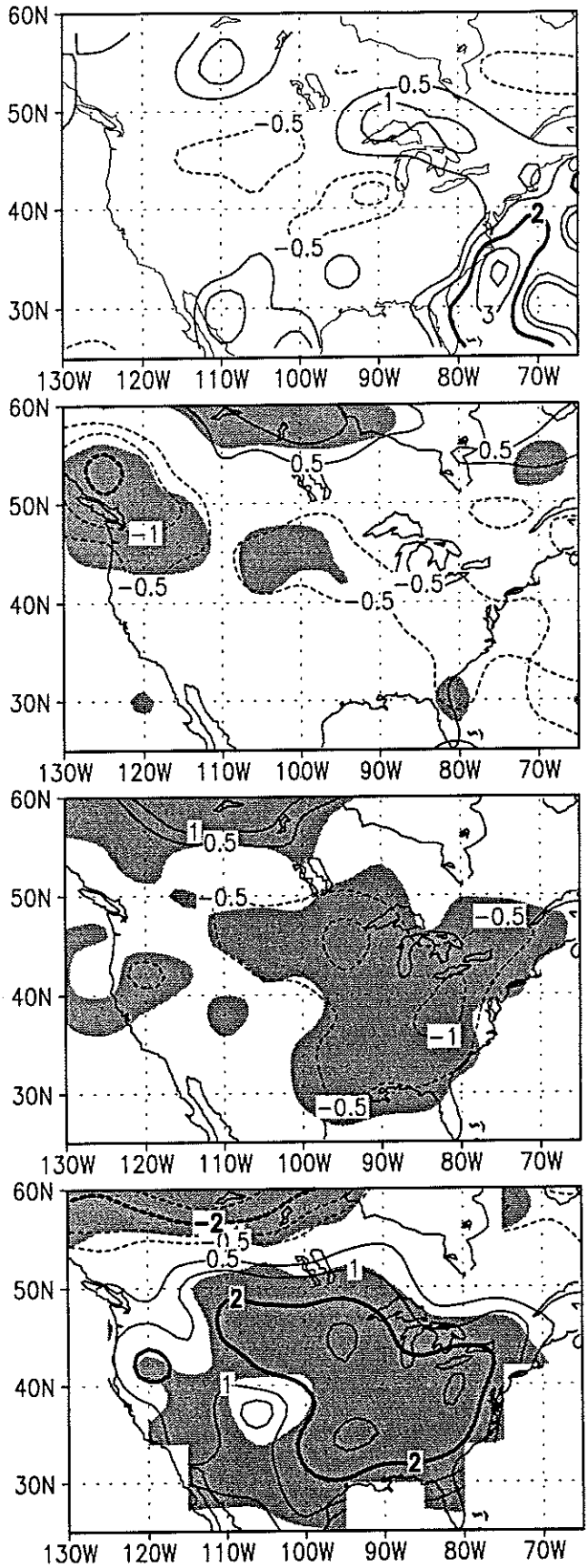
60N
50N
40N
30N
130W 120W 110W 100W 90W 80W 70W
0.5
1
-0.5
2
3
(a)
-1
(b)
(c)
-2
1.5
(d)

Figure 14

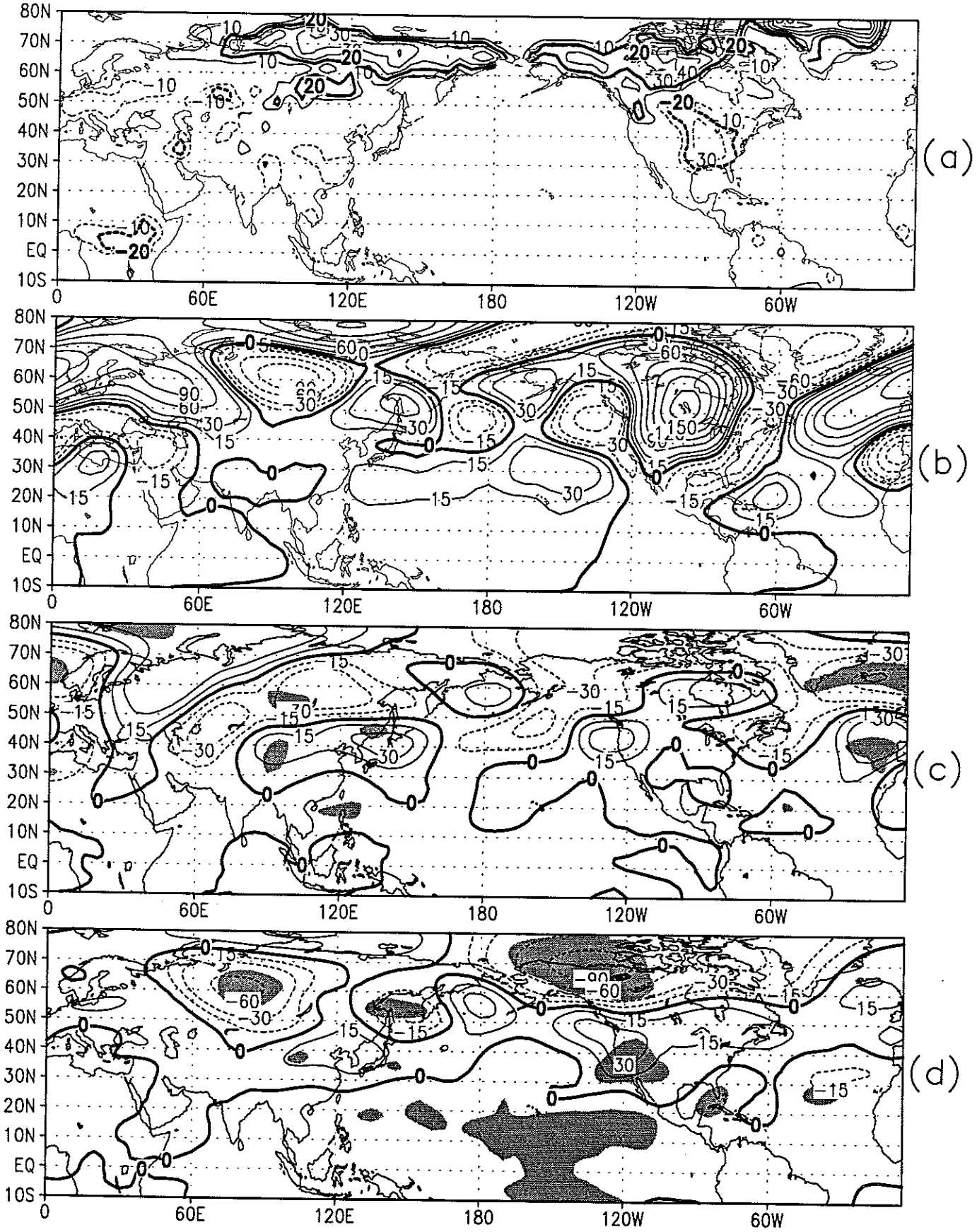
80N
70N
60N
50N
40N
30N
20N
10N
EQ
10S
0
60E
120E
180
120W
60W
(a)
(b)
(c)
(d)